JRC Scientific and Technical Reports

Linear Model of a Pseudo-Dynamic Testing System

F. J. Molina, G. Magonette and B. Viaccoz

European Commission, Joint Research Centre, IPSC, ELSA Laboratory
Via E. Fermi 2749, TP 480, I-21027 Ispra (VA), Italy

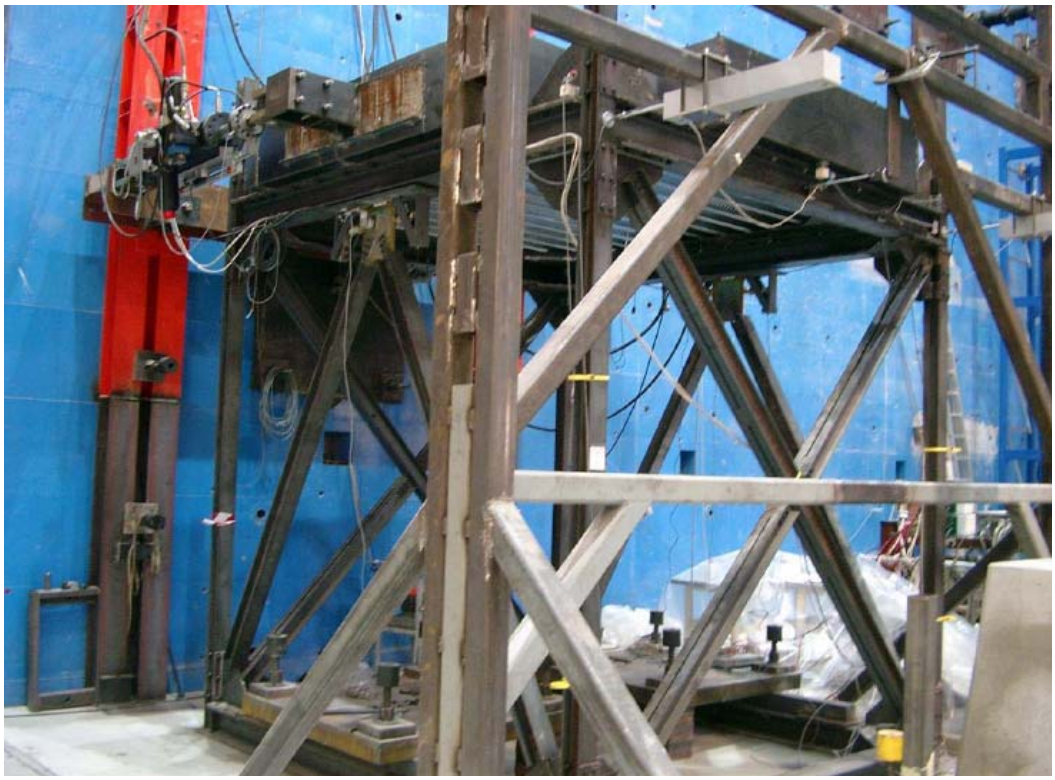

EUR 24313 EN - 2010

JRC EUROPEAN COMMISSION

ipsc Institute for the Protection and Security of the Citizen

The mission of the JRC-IPSC is to provide research results and to support EU policy-makers in their effort towards global security and towards protection of European citizens from accidents, deliberate attacks, fraud and illegal actions against EU policies.

European Commission
Joint Research Centre
Institute for the Protection and Security of the Citizen

Contact information
Address: Francisco J. Molina
E-mail: francisco.molina@jrc.ec.europa.eu
Tel.: +39 0332 786069
Fax: +39 0332 789049

http://ipsc.jrc.ec.europa.eu/
http://www.jrc.ec.europa.eu/

JRC 57549

EUR 24313 EN
ISSN 1018-5593
ISBN 978-92-79-15125-5
DOI 10.2788/82843

Luxembourg: Office for Official Publications of the European Union

Printed in Italy

Linear Model of a Pseudo-Dynamic Testing System

F. J. Molina, G. Magonette and B. Viaccoz

European Commission, JRC, IPSC, ELSA laboratory, I-21027 Ispra (VA),Italy

ABSTRACT

A linear analytical N-DoF model of a complete pseudo-dynamic testing system is developed and calibrated by means of comparison with experimental results. The model is formulated as a state space equation system by assembling the respective equations for the hydraulic actuators, control law, specimen and testing method. For the case of a 1-DoF steel frame specimen, the control characteristics are experimentally obtained and used for the tuning of the parameters of the model. This model can be useful for understanding and quantitatively predicting distortions of the pseudo-dynamic response due to the presence of control errors as well as for simulating alternative testing methods.

1 INTRODUCTION

The European Laboratory for Structural Assessment (ELSA) of the JRC of the EC counts with almost two decades of experience on structural testing and most of the performed experiments have been done on large size specimens submitted to earthquake loading by means of the pseudo-dynamic (PsD) method. ELSA has contributed to the development of the PsD method with many improvements and extensions of its applicability (Molina and Géradin, 2007) and has developed the hardware and software that implement them (Pegon et al., 2008).

Independently of these improvements in the testing method, the importance of limiting control errors for the quality of the test has been recognised from the first studies (Shing and Mahin, 1987) and we have developed analytical and experimental tools for understanding and quantifying their effects (Molina et al., 2002, Vidal, 2005). An step forward is done with the present work, by developing an analytical linear model of the control system, the testing specimen and the testing set-up for the continuous PsD test (Magonette et al., 1998) which is the preferred testing technique currently at ELSA.

The proposed model is applicable in an approximate manner to hydraulic actuators with Proportional-Integral-Derivative (PID) controllers (Phillips and Harbor, 1999) that may also include feed-forward and differential-pressure gains. Since the real specimen should be non linear and the hydraulic devices are intrinsically non linear (Ziaei & Sepehri, 2000, Knohl & Unbehauen, 2000, Plummer 2008), the linearity will be an acceptable assumption only for small amplitudes of the movement around a working position. The principles underlying the state-space formulation of this model are similar to those of the Laplace-domain model formulated by Conte & Trombetti (2000) or by Plummer (2008) in its linear version, except for the use in this study of an additional damping parameter inside the actuator.

This report contains the state-space linear formulation of the analytical model including the actuators, specimen, controller and testing method; firstly, for a 1-DoF system and,

secondly, for a system with several DoFs and several actuators. Then, taking as specimen in the ELSA laboratory a 1-DoF frame controlled by two actuators, experimental frequency response functions FRFs of the control system were obtained by using sine chirp testing and these experimental curves were used to successfully calibrate the analytical model.

2 ANALYTICAL MODEL

In this chapter the linear model for the control system and the PsD testing set-up is formulated by writing its equations in the state space. This model assumes that one actuator or more are used to control the displacement at each one of the DoFs considered for the specimen as is typical for a PsD testing set-up. In order to start with the simplest, the first two sections of this chapter deal only with the case of a 1-DoF system.

2.1 Model of the control system for a 1-DoF specimen

This section develops an analytical linear model for the control system of a 1-DoF specimen using one actuator. ***Figure 1*** shows a schematic representation of the model. The equations regarding the servo-valve, the actuator, the specimen and the controller are formulated in separated subsections.

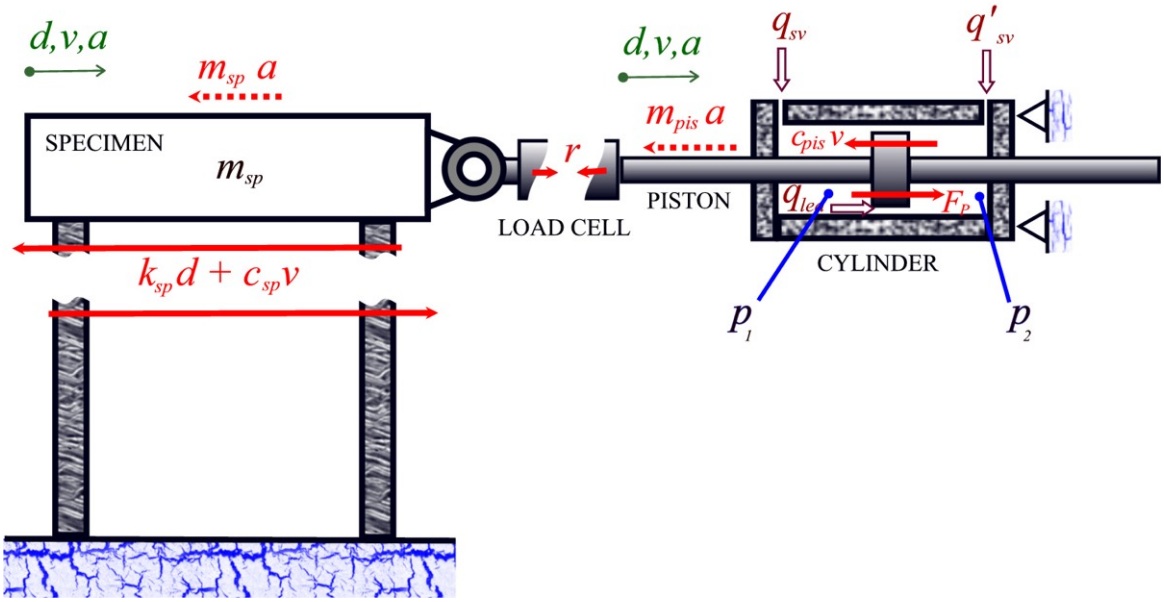

Figure 1. Model of the control system.

2.1.1 Servo-valve model

For PsD tests, the frequencies of concern for accuracy purposes at the control system are much lower than for shaking-table or real-time tests. It is worth to mention that, working with reduced flow rates (far from the capacity of the servo-valve), the resonance frequency of the relatively small servo-valves used for PsD testing uses to be larger than 50 Hz. Then, the only effect of the non proportionality at the servo-valve that can be important to consider in a typical PsD set-up is a possible slight reduction of the stability margin due to a small phase lag (a few degrees) already visible at the maximum frequency of the operating range of the control, which is normally lower than 10 Hz.

This fact allows considering within this model the typical four-way proportional servo-valve of an actuator as a perfectly proportional device without any delay by using an equation of the type

$$q_{SV}(t) = k_{SV}\, x_{SV}(t) \tag{1}$$

where $q_{SV}(t)$ is the servo-valve oil flow rate (volume per time unit) as a function of time t, k_{SV} is the servo-valve flow-gain coefficient (assumed constant in this model) and $x_{SV}(t)$ is the electric input command to the servo-valve sent by the controller. If this flow (1) is positive, it is the one going in into the first chamber (left chamber in ***Figure 1***) and we will assume it to be equal to the one going out of the second chamber

$$-q'_{SV}(t) = k_{SV}\, x_{SV}(t) \tag{2}$$

In a non-linear model, k_{SV} would be proportional to the square root of the pressure jump (e.g., Plummer 2008). However, since our model is linear and studies the oscillations around an equilibrium position, at which there is no force in the piston, we will consider here that the pressure in both chambers at that equilibrium position is approximately the average between the ones at the high and at the low pressure lines connected to the servo-valve. Hence, the input and output pressure jumps are almost equal and can be assumed constant if the pressure oscillations in the chambers are small and, consequently, k_{SV} in (1) and (2) is also a constant. If $q_{SV}(t)$ is negative, the oil is getting out of the first chamber and getting in into the second one, but anyway the flow rates always follow equations (1) and (2).

2.1.2 Cylinder-piston model

Within this model, the servo-valve flow rate (1) entering in the pulling chamber of the symmetric cylinder (chamber on the left in **Figure 1**) is assumed to obey the flow continuity equation

$$q_{SV}(t) = q_{vel}(t) + q_{lea}(t) + q_{com}(t) \tag{3}$$

which means that the flux is employed, firstly, in moving the piston, secondly in compensating for the leakage to the other chamber and, thirdly, in compensating for the oil compressibility. The first addend is equal to the rate of volume change in that chamber due to the piston velocity

$$q_{vel}(t) = Av(t) \tag{4}$$

being A the piston area and $v(t)$ the velocity of the piston with respect to the fixed cylinder

$$v(t) = \frac{d}{dt} d(t) = \dot{d}(t) \tag{5}$$

where $d(t)$ is the associated displacement of the piston.

Successively, the second addend in (3) reflects the leakage flow between the piston and the cylinder from one chamber to the other. Within this model, such flow is considered laminar and then proportional to the pressure difference between the chambers

$$\Delta P(t) = p_1(t) - p_2(t) \tag{6}$$

through a constant leakage coefficient c_{lea}. That is to say,

$$q_{lea}(t) = c_{lea}\Delta P(t) = \frac{c_{lea}}{A} F_P(t) \tag{7}$$

where

$$F_P(t) = A\Delta P(t) \tag{8}$$

is the total pulling hydraulic force of the oil pressure acting on the symmetric piston.

Finally, the third addend in (3) represents the flow required to compensate for the volume change rate associated to the fluid compressibility

$$q_{com}(t) = (\dot{V}_1(t))_{com} \tag{9}$$

Such compressibility is governed by the effective bulk modulus of the oil β that is assumed constant and relates the change of pressure in the chamber with the change of specific volume of the mass of oil contained in it

$$\beta = \frac{\dot{p}_1}{(\dot{V}_1(t))_{com} / V_1} \tag{10}$$

Where, for linearization, the reference volume of the first chamber V_1 is assumed constant in this formula. Then, for the flow rate (3) entering into the first chamber, we have

$$q_{SV}(t) = Av(t) + \frac{c_{lea}}{A} F_P(t) + \frac{V_1}{\beta} \dot{p}_1(t) \tag{11}$$

while for the second chamber it is

$$q'_{SV}(t) = -Av(t) - \frac{c_{lea}}{A} F_P(t) + \frac{V_2}{\beta} \dot{p}_2(t) \tag{12}$$

Now, because of (1) and (2)

$$q_{SV}(t) + q'_{SV}(t) = 0 \tag{13}$$

and, by substituting (11) and (12)

$$V_1 \dot{p}_1(t) + V_2 \dot{p}_2(t) = 0 \tag{14}$$

Also, from (6) and (8),

$$\dot{p}_1(t) - \dot{p}_2(t) = \frac{\dot{F}_P}{A} \tag{15}$$

and, by combining (14) and (15),

$$\dot{p}_1(t) = \frac{V_2}{V_1 + V_2} \frac{\dot{F}_P}{A} \tag{16}$$

$$\dot{p}_2(t) = -\frac{V_1}{V_1 + V_2} \frac{\dot{F}_P}{A}$$

By introducing (16) into (11), it is derived that

$$q_{SV}(t) = Av(t) + \frac{c_{lea}}{A} F_P(t) + \frac{V_1 V_2}{V_1 + V_2} \frac{\dot{F}_P(t)}{\beta A} \tag{17}$$

Since the hydraulic force will be chosen as a state variable in our formulation, eq. (17) is rewritten as

$$\dot{F}_P(t) = k_{oil} \left[\frac{q_{SV}(t)}{A} - v(t) \right] - \frac{1}{\tau_{lea}} F_P(t) \tag{18}$$

where the total stiffness of the oil columns contained in the cylinder chambers is

$$k_{oil} = \frac{\beta A}{V_1 / A} + \frac{\beta A}{V_2 / A} = \frac{(V_1 + V_2)\beta A^2}{V_1 V_2} \tag{19}$$

Or, in the particular case of using the centre of the piston run as reference (where the volumes of both chambers are equal)

$$\left(k_{oil}\right)_{centre} = \frac{\left(\frac{V}{2} + \frac{V}{2}\right)\beta A^2}{\frac{V}{2}\frac{V}{2}} = \frac{4\beta A^2}{V} \tag{20}$$

where

$$V = V_1 + V_2 \tag{21}$$

The second constant introduced in (18)

$$\tau_{lea} = \frac{A^2}{k_{oil} c_{lea}} \tag{22}$$

is the time characteristic associated to the force decay due to the oil leakage between the chambers. In fact, in case of a piston with blocked movement ($v = 0$) and with its servo-valve closed ($q_{SV} = 0$), the force law solved from (18) would be

$$F_P(t) = F_P(0)\, e^{-\frac{t}{\tau_{lea}}} \tag{23}$$

2.1.3 Specimen model

For the case of a 1-DoF specimen, the equilibrium equation of the addition of the free body relating to the specimen mass and the free body relating to the piston (**Figure 1**) is in total

$$(m_{sp} + m_{pis})a(t) + (c_{sp} + c_{pis})v(t) + k_{sp} d(t) = F_P(t) \tag{24}$$

where m_{sp} is the specimen mass (including the attachment to the piston up to the load cell for this model), c_{sp} is an equivalent viscous damping coefficient to model approximately all possible kinds of damping of the specimen and k_{sp} is its stiffness. Also in (24), c_{pis} is a viscous damping coefficient that models the friction of the piston with the cylinder, m_{pis} is the mass of the piston up at the level of its load cell and the acceleration is

$$a(t) = \dot{v}(t) \tag{25}$$

By considering (25), equation (24) can be rewritten in a more convenient way as

$$\dot{v}(t) = (m_{sp} + m_{pis})^{-1} \left[F_P(t) - (c_{sp} + c_{pis})v(t) - k_{sp} d(t) \right] \tag{26}$$

in order to prepare it for the state-space formulation.

2.1.4 Controller model

Even though the controllers used nowadays are digital in most of the cases, within this model the controller algorithm will be approximated by a time-continuous law. More precisely, we will assume a displacement-control PID algorithm with additional gains of feed-forward and differential pressure, that is to say, the command signal computed at the controller of each piston is

$$c_{con}(t) = k_P \left[\varepsilon(t) + k_I^{-1} \int_t \varepsilon(t) + k_D \dot{\varepsilon}(t) + k_{FF} v_r(t) + k_{\Delta P} \Delta P(t) \right] \tag{27}$$

where k_P, k_I, k_D, k_{FF} and $k_{\Delta P}$ are respectively the proportional, integral, derivative, feed-forward and differential-pressure gains. The error signal that appears in (27) is

computed as the difference between the reference (target) displacement $d_r(t)$ and the measured displacement

$$\varepsilon(t) = d_r(t) - d(t) \tag{28}$$

Also in (27) the reference velocity is

$$v_r(t) = \dot{d}_r(t) \tag{29}$$

Afterwards, the servo-valve electric command contained in (1) is generated as

$$x_{SV}(t) = k_{con}\, c_{con}(t) \tag{30}$$

where k_{con} is the output sensitivity of the controller.

2.1.5 State-space formulation of the whole control system

As a preparation to the formulation of the state equations, equations (1), (8), (27), (28) and (30) can be combined in the form

$$\begin{aligned} &\frac{q_{SV}(t)}{A} = \frac{k_{SV}}{A} x_{SV}(t) = \frac{k_{SV} k_{con}}{A} c_{con}(t) \\ &= k_{v-c} k_P \left[d_r(t) - d(t) + k_I^{-1} \varepsilon_I(t) + k_D \left(v_r(t) - v(t) \right) + k_{FF} v_r(t) + \frac{k_{\Delta P}}{A} F_P(t) \right] \end{aligned} \tag{31}$$

where

$$\varepsilon_I(t) = \int_t \varepsilon(t) \tag{32}$$

or, equivalently,

$$\dot{\varepsilon}_I(t) = \varepsilon(t) = d_r(t) - d(t) \tag{33}$$

Also in (31), for abbreviation,

$$k_{v-c} = \frac{k_{SV} k_{con}}{A} \tag{34}$$

is the servo-valve gain expressed in piston velocity units divided by the units of $c_{con}(t)$.

Then, by substituting (31) in (18),

$$\begin{aligned} \dot{F}_P(t) = k_{oil} \Big\{ & k_{v-c} k_P \Big[d_r(t) - d(t) + k_I^{-1} \varepsilon_I(t) + k_D \left(v_r(t) - v(t) \right) \\ & + k_{FF} v_r(t) + k_{\Delta P} A^{-1} F_P(t) \Big] - v(t) \Big\} - \tau_{lea}^{-1} F_P(t) \end{aligned} \tag{35}$$

The standard form of the state equations of a linear time-invariant analogue system is given by (Phillips and Harbor, 1999)

$$\begin{aligned} \dot{\mathbf{x}}(t) &= \mathbf{A}\mathbf{x}(t) + \mathbf{B}\mathbf{u}(t) \\ \mathbf{y}(t) &= \mathbf{C}\mathbf{x}(t) + \mathbf{D}\mathbf{u}(t) \end{aligned} \tag{36}$$

where $\mathbf{x}(t)$ is the state vector containing the state variables and $\mathbf{u}(t)$ and $\mathbf{y}(t)$ are the input and output vectors respectively. The matrices $\mathbf{A}$, $\mathbf{B}$, $\mathbf{C}$ and $\mathbf{D}$ contain constant coefficients.

In order to express the model of the control system into state equations, we will define the state equation

$$\dot{\mathbf{x}}_{cs}(t) = \mathbf{A}_{cs}\mathbf{x}_{cs}(t) + \mathbf{B}_{cs}\mathbf{u}_{cs}(t) \tag{37}$$

where, by choice,

$$\mathbf{x}_{cs}(t) = \begin{bmatrix} d(t) \\ v(t) \\ F_P(t) \\ \varepsilon_I(t) \end{bmatrix} \quad ; \quad \mathbf{u}_{cs}(t) = \begin{bmatrix} d_r(t) \\ v_r(t) \end{bmatrix} \tag{38}$$

Are, respectively, the state and input vectors of the control system model.

The coefficients of the matrices in (37) are derived in row-order from expressions (5), (26), (35) and (33) as

$$\mathbf{A}_{cs} = \begin{bmatrix} 0 & 1 & 0 & 0 \\ -(m_{sp}+m_{pis})^{-1}k_{sp} & -(m_{sp}+m_{pis})^{-1}(c_{sp}+c_{pis}) & (m_{sp}+m_{pis})^{-1} & 0 \\ -k_{oil}k_{v-c}k_P & -k_{oil}(k_{v-c}k_Pk_D+1) & k_{oil}k_{v-c}k_Pk_{\Delta P}A^{-1}-\tau_{lea}^{-1} & k_{oil}k_{v-c}k_Pk_I^{-1} \\ -1 & 0 & 0 & 0 \end{bmatrix}$$

$$\mathbf{B}_{cs} = \begin{bmatrix} 0 & 0 \\ 0 & 0 \\ k_{oil}k_{v-c}k_P & k_{oil}k_{v-c}k_P(k_D+k_{FF}) \\ 1 & 0 \end{bmatrix} \tag{39}$$

2.2 Model of the pseudo-dynamic testing set-up

Within this model, for the 1-DoF specimen, the PsD simulation will consist of the integration of the equation of motion

$$m_{PsD}\frac{d^2}{dT^2}d_r(T) + c_{PsD}\frac{d}{dT}d_r(T) + r(T) = f_{INP}(T) \tag{40}$$

where the displacement $d_r(T)$ is solved and used as reference for the control system and the restoring force $r(T)$ is directly measured at the piston load cell (***Figure 1***). Within equation (40), in some cases, the values of the theoretical mass m_{PsD} and viscous damping c_{PsD} of the specimen may differ from the physical ones m_{sp} and c_{sp} (***Figure 1***). In the case of seismic load, the external input force is defined as

$$f_{INP}(T) = -m_{PsD} a_g(T) \tag{41}$$

where $a_g(T)$ is the specified ground accelerogram. In equations (40) and (41) the time variable is the prototype time T, which is the original time concerning the earthquake and normally lasts for a few tens of seconds. However, the real time t for the execution of the test in the laboratory may last for several hours. In most of the cases the time scale factor, defined as the proportion between the experiment time and the prototype time

$$\lambda = \frac{t}{T} \tag{42}$$

is a constant during the PsD test and may range from 10 to 1000.

Equation (40) is solved step by step normally by an explicit method so that the solved displacement is imposed (using it as controller reference) to the specimen and the value of the experimental force measured at the load cell is used for integrating the next step in the equation. When using a time increment small enough, the errors induced by the numeric integration can be disregarded as it is the case for the continuous PsD method normally used at ELSA (Pegon et al., 2008) and, thus, the continuous solution of the equation (40) will be directly used in the current model.

In order to couple the PsD equation of motion (40) with the developed model of the control system, the equation will be translated to the experiment time by having in account (42) and working out

$$\frac{d}{dT} d_r = \frac{dt}{dT}\left(\frac{d}{dt} d_r\right) = \lambda \dot{d}_r = \lambda v_r \tag{43}$$

where definition (29) has been applied, and

$$\frac{d}{dT}\left[\frac{d}{dT} d_r\right] = \frac{d}{dT}\left[\lambda v_r\right] = \frac{dt}{dT}\left[\frac{d}{dt}\left(\lambda v_r\right)\right] = \lambda\left[\lambda \dot{v}_r\right] \tag{44}$$

Then, by substituting (43) and (44) in (40),

$$m_{PsD}\lambda^2 \dot{v}_r(t) + c_{PsD}\lambda v_r(t) + r(t) = f_{INP}(t) \tag{45}$$

which can also be expressed as

$$\begin{aligned}\dot{v}_r(t) &= \lambda^{-2} m_{PsD}^{-1}\left[\, f_{INP}(t) - c_{PsD}\lambda v_r(t) - r(t)\right] \\ &= \lambda^{-2} m_{PsD}^{-1}\Big[\quad f_{INP}(t) - c_{PsD}\lambda v_r(t) - m_{sp}\left(m_{sp}+m_{pis}\right)^{-1} F_P(t) \\ &+\left(m_{sp}\left(m_{sp}+m_{pis}\right)^{-1}\left(c_{sp}+c_{pis}\right) - c_{sp}\right)v(t) \\ &+\left(m_{sp}\left(m_{sp}+m_{pis}\right)^{-1} - 1\right)k_{sp}d(t) \quad\Big]\end{aligned} \tag{46}$$

In order to pass from expression (45) to (46), by dynamic equilibrium of the specimen mass in ***Figure 1***, the restoring force has been expressed as

$$r(t) = m_{sp}a(t) + c_{sp}v(t) + k_{sp}d(t) \tag{47}$$

and, by introducing equations (25) and (26),

$$\begin{aligned}r(t) &= m_{sp}\left(m_{sp}+m_{pis}\right)^{-1}\left[\, F_P(t) - \left(c_{sp}+c_{pis}\right)v(t) - k_{sp}d(t)\right] + c_{sp}v(t) + k_{sp}d(t) \\ &= m_{sp}\left(m_{sp}+m_{pis}\right)^{-1} F_P(t) + \left(c_{sp} - m_{sp}\left(m_{sp}+m_{pis}\right)^{-1}\left(c_{sp}+c_{pis}\right)\right)v(t) \\ &+\left(1 - m_{sp}\left(m_{sp}+m_{pis}\right)^{-1}\right)k_{sp}d(t)\end{aligned} \tag{48}$$

Now, the state equation for the PsD test using the control system developed in the previous section, is

$$\dot{\mathbf{x}}(t) = \mathbf{A}\mathbf{x}(t) + \mathbf{B}\mathbf{u}(t) \tag{49}$$

where, by choice,

$$\mathbf{x}(t) = \begin{bmatrix} d_r(t) \\ v_r(t) \\ d(t) \\ v(t) \\ F_P(t) \\ \varepsilon_I(t) \end{bmatrix} \quad ; \quad \mathbf{u}(t) = \left[\, f_{INP}(t)\right] \tag{50}$$

are the state and input vectors respectively.

In this case, the coefficients of the matrices in (49) are derived in row-order from expressions (29), (46), (5), (26), (35) and (33) respectively as

$$\mathbf{A}=\begin{bmatrix} 0 & 1 & 0 \\ 0 & -\lambda^{-1}m_{PsD}^{-1}c_{PsD} & -\lambda^{-2}m_{PsD}^{-1}m_{pis}(m_{sp}+m_{pis})^{-1}k_{sp} \\ 0 & 0 & 0 \\ 0 & 0 & -(m_{sp}+m_{pis})^{-1}k_{sp} \\ k_{oil}k_{v-c}k_P & k_{oil}k_{v-c}k_P(k_D+k_{FF}) & -k_{oil}k_{v-c}k_P \\ 1 & 0 & -1 \end{bmatrix}$$

$$\begin{bmatrix} 0 & 0 & 0 \\ \lambda^{-2}m_{PsD}^{-1}\left(m_{sp}(m_{sp}+m_{pis})^{-1}(c_{sp}+c_{pis})-c_{sp}\right) & -\lambda^{-2}m_{PsD}^{-1}m_{sp}(m_{sp}+m_{pis})^{-1} & 0 \\ 1 & 0 & 0 \\ -(m_{sp}+m_{pis})^{-1}(c_{sp}+c_{pis}) & (m_{sp}+m_{pis})^{-1} & 0 \\ -k_{oil}(k_{v-c}k_Pk_D+1) & k_{oil}k_{v-c}k_Pk_{\Delta P}A^{-1}-\tau_{lea}^{-1} & k_{oil}k_{v-c}k_Pk_I^{-1} \\ 0 & 0 & 0 \end{bmatrix}$$

$$\mathbf{B}=\begin{bmatrix} 0 \\ \lambda^{-2}m_{PsD}^{-1} \\ 0 \\ 0 \\ 0 \\ 0 \end{bmatrix} \tag{51}$$

2.3 Generalisation to a N-DoF specimen and formulation of the global state-space model

In this section the case of a PsD experiment on a N-DoF specimen will be considered. The PsD equations of motion will be based on those N DoFs and the equations relating the control will refer to M actuators. The number of actuators must be larger than the number of DoFs

$$M \geq N \tag{52}$$

so that they can impose any computed displacement vector on the specimen.

For the dynamic model of the specimen we will consider the same DoFs as for the PsD equations and, similarly to (47), having as dynamic equilibrium the equations

$$\mathbf{m}_{sp}\mathbf{a}_{sp}(t)+\mathbf{c}_{sp}\mathbf{v}_{sp}(t)+\mathbf{k}_{sp}\mathbf{d}_{sp}(t)=\mathbf{r}_{sp}(t) \tag{53}$$

where $\mathbf{a}_{sp}$, $\mathbf{v}_{sp}$, $\mathbf{d}_{sp}$ and $\mathbf{r}_{sp}$ are respectively the acceleration, velocity, displacement and restoring force vectors of the specimen and $\mathbf{m}_{sp}$, $\mathbf{c}_{sp}$ and $\mathbf{k}_{sp}$, are respectively its matrices of mass, damping and stiffness.

2.3.1 Formulation of the control system

Within this model, the displacements of the pistons $\mathbf{d}_{pis}$ inside of their cylinders will be geometrically determined by the ones of the specimen through the linear relation

$$\mathbf{d}_{pis}(t) = \mathbf{T}\mathbf{d}_{sp}(t) \tag{54}$$

where $\mathbf{T}$ is a constant transformation matrix which is also used within the PsD algorithm to convert the computed reference displacements of the specimen $\mathbf{d}^r_{sp}(t)$ into the reference ones of the pistons

$$\mathbf{d}^r_{pis}(t) = \mathbf{T}\mathbf{d}^r_{sp}(t) \tag{55}$$

or

$$\mathbf{v}^r_{pis}(t) = \dot{\mathbf{d}}^r_{pis}(t) = \mathbf{T}\mathbf{v}^r_{sp}(t) \tag{56}$$

in the derivative form, with

$$\mathbf{v}^r_{sp}(t) = \dot{\mathbf{d}}^r_{sp}(t) \tag{57}$$

This means that, for simplification, the reaction system of the pistons and their couplings have been modelled as infinitely rigid.

In the same way, the velocities and accelerations of the pistons are determined by the derivative of expression (54) as

$$\mathbf{v}_{pis}(t) = \dot{\mathbf{d}}_{pis}(t) = \mathbf{T}\mathbf{v}_{sp}(t) \tag{58}$$

and

$$\mathbf{a}_{pis}(t) = \dot{\mathbf{v}}_{pis}(t) = \mathbf{T}\mathbf{a}_{sp}(t) \tag{59}$$

respectively, where, by definition,

$$\mathbf{v}_{sp}(t) = \dot{\mathbf{d}}_{sp}(t) \tag{60}$$

and

$$\mathbf{a}_{sp}(t) = \dot{\mathbf{v}}_{sp}(t) \tag{61}$$

We will assume that the load cells of the pistons measure their force at the same position and direction of the piston displacement. Then, by reciprocity, the generalised restoring forces at the DoFs of the specimen, which appear at the right side of equation (53), are obtained from the forces at the load cells of the pistons $\mathbf{r}_{pis}$ by using the transposed matrix

$$\mathbf{r}_{sp}(t) = \mathbf{T}^T\mathbf{r}_{pis}(t) \tag{62}$$

By free-body equilibrium, the load cell forces can be written as a function of the other forces acting on the pistons (***Figure 1***)

$$\mathbf{r}_{pis}(t) = \mathbf{F}_P(t) - \mathbf{m}_{pis}\mathbf{a}_{pis}(t) - \mathbf{c}_{pis}\mathbf{v}_{pis}(t) \tag{63}$$

where $\mathbf{F}_P$, $\mathbf{m}_{pis}$ and $\mathbf{c}_{pis}$ are respectively the vector of hydraulic forces on the pistons and the diagonal piston matrices of mass and internal damping.

Then, by introducing (62), (63), (58) and (59) in (53),

$$\mathbf{m}_{sp}\mathbf{a}_{sp}(t) + \mathbf{c}_{sp}\mathbf{v}_{sp}(t) + \mathbf{k}_{sp}\mathbf{d}_{sp}(t) = \mathbf{T}^T\left[\mathbf{F}_P(t) - \mathbf{m}_{pis}\mathbf{T}\mathbf{a}_{sp}(t) - \mathbf{c}_{pis}\mathbf{T}\mathbf{v}_{sp}(t)\right] \tag{64}$$

or, equivalently,

$$\left(\mathbf{m}_{sp} + \mathbf{T}^T\mathbf{m}_{pis}\mathbf{T}\right)\mathbf{a}_{sp}(t) + \left(\mathbf{c}_{sp} + \mathbf{T}^T\mathbf{c}_{pis}\mathbf{T}\right)\mathbf{v}_{sp}(t) + \mathbf{k}_{sp}\mathbf{d}_{sp}(t) = \mathbf{T}^T\mathbf{F}_P(t) \tag{65}$$

which, by introducing (61), allows to arrive at a similar expression to (26)

$$\dot{\mathbf{v}}_{sp}(t) = \left(\mathbf{m}_{sp} + \mathbf{T}^T\mathbf{m}_{pis}\mathbf{T}\right)^{-1}\left[\mathbf{T}^T\mathbf{F}_P(t) - \left(\mathbf{c}_{sp} + \mathbf{T}^T\mathbf{c}_{pis}\mathbf{T}\right)\mathbf{v}_{sp}(t) - \mathbf{k}_{sp}\mathbf{d}_{sp}(t)\right] \tag{66}$$

After these relations have been introduced, we will also generalise some other equations of the 1-DoF model in order to arrive at the state space formulation for the N-DoF case. For example, equation (1) will be transformed into

$$\mathbf{q}_{SV}(t) = \mathbf{k}_{SV}\mathbf{x}_{SV}(t) \tag{67}$$

where $\mathbf{q}_{sv}$ and $\mathbf{x}_{sv}$ are respectively the vectors of flow rates and commands of the servo-valves and $\mathbf{k}_{sv}$ is the diagonal matrix flow-gain coefficients, having that

$$\mathbf{x}_{SV}(t) = \mathbf{k}_{con}\,\mathbf{c}_{con}(t) \tag{68}$$

where $\mathbf{k}_{con}$ is the diagonal matrix of output sensitivities of the controller.

The controller commands calculated through the control algorithm will be written in vector form as

$$\mathbf{c}_{con}(t) = \mathbf{k}_P\left[\boldsymbol{\varepsilon}(t) + \mathbf{k}_I{}^{-1}\boldsymbol{\varepsilon}_I(t) + \mathbf{k}_D\,\dot{\boldsymbol{\varepsilon}}(t) + \mathbf{k}_{FF}\mathbf{v}^r_{pis}(t) + \mathbf{k}_{\Delta P}\boldsymbol{\Delta}\mathbf{P}(t)\right] \tag{69}$$

where $\mathbf{k}_P$, $\mathbf{k}_I$, $\mathbf{k}_D$, $\mathbf{k}_{FF}$ and $\mathbf{k}_{\Delta P}$ are respectively the matrices containing the proportional, integral, derivative, feed-forward and differential-pressure gains and $\boldsymbol{\Delta}\mathbf{P}$ is the vector of pressure differences. The error signal vector is computed as the difference between the reference (target) displacement $\mathbf{d}^r_{pis}(t)$ and the measured displacement $\mathbf{d}_{pis}(t)$

$$\boldsymbol{\varepsilon}(t) = \mathbf{d}^r_{pis}(t) - \mathbf{d}_{pis}(t) = \mathbf{T}\mathbf{d}^r_{sp}(t) - \mathbf{T}\mathbf{d}_{sp}(t) \tag{70}$$

Where (54) and (55) have also been used and

$$\dot{\boldsymbol{\varepsilon}}(t) = \mathbf{v}_{pis}^{r}(t) - \mathbf{v}_{pis}(t) \tag{71}$$

Similarly to equation (33), the derivative of the vector of the integrated control errors at the different actuators will be expressed as

$$\dot{\boldsymbol{\varepsilon}}_{I}(t) = \boldsymbol{\varepsilon}(t) = \mathbf{T}\mathbf{d}_{sp}^{r}(t) - \mathbf{T}\mathbf{d}_{sp}(t) \tag{72}$$

where (70) has been used.

By applying expression (18) to each one of the actuators and using a matrix form,

$$\dot{\mathbf{F}}_{P}(t) = \mathbf{k}_{oil}\left[\mathbf{A}_{pis}^{-1}\mathbf{q}_{SV}(t) - \mathbf{v}_{pis}(t)\right] - \boldsymbol{\tau}_{lea}^{-1}\,\mathbf{F}_{P}(t) \tag{73}$$

which using (67), (68), (69), (70), (71), (56) and (58) can be transformed into

$$\begin{aligned}\dot{\mathbf{F}}_{P}(t) = \mathbf{k}_{oil}\Big\{\mathbf{k}_{v-c}\mathbf{k}_{P}\Big[\mathbf{T}\left(\mathbf{d}_{sp}^{r}(t) - \mathbf{d}_{sp}(t)\right) + \mathbf{k}_{I}^{-1}\boldsymbol{\varepsilon}_{I}(t) + \mathbf{k}_{D}\mathbf{T}\left(\mathbf{v}_{sp}^{r}(t) - \mathbf{v}_{sp}(t)\right)\\ + \mathbf{k}_{FF}\mathbf{T}\mathbf{v}_{sp}^{r}(t) + \mathbf{k}_{\Delta P}\mathbf{A}_{pis}^{-1}\mathbf{F}_{P}(t)\Big] - \mathbf{T}\mathbf{v}_{sp}(t)\Big\} - \boldsymbol{\tau}_{lea}^{-1}\,\mathbf{F}_{P}(t)\end{aligned} \tag{74}$$

where, by definition,

$$\mathbf{k}_{v-c} = \mathbf{A}_{pis}^{-1}\mathbf{k}_{SV}\mathbf{k}_{con} \tag{75}$$

and

$$\mathbf{F}_{P}(t) = \mathbf{A}_{pis}\Delta\mathbf{P}(t) \tag{76}$$

Being $\mathbf{F}_P$ the vector of hydraulic force on the pistons and $\mathbf{k}_{oil}$, $\mathbf{A}_{pis}$ and $\boldsymbol{\tau}_{lea}$ respectively the diagonal matrices of oil column stiffness, piston sections and leakage time parameters.

We will express the model of the control system into the state equations

$$\dot{\mathbf{x}}_{cs}(t) = \mathbf{A}_{cs}\mathbf{x}_{cs}(t) + \mathbf{B}_{cs}\mathbf{u}_{cs}(t) \tag{77}$$

where, by choice,

$$\mathbf{x}_{cs}(t) = \begin{bmatrix}\mathbf{d}_{sp}(t)\\ \mathbf{v}_{sp}(t)\\ \mathbf{F}_{P}(t)\\ \boldsymbol{\varepsilon}_{I}(t)\end{bmatrix} \quad ; \quad \mathbf{u}_{cs}(t) = \begin{bmatrix}\mathbf{d}_{sp}^{r}(t)\\ \mathbf{v}_{sp}^{r}(t)\end{bmatrix} \tag{78}$$

are the state and input vectors respectively.

The coefficients of the matrices in (77) are derived by row-order from expressions (60), (66), (74) and (72) as

$$\mathbf{A}_{cs}=\begin{bmatrix} \mathbf{0} & \mathbf{I} \\ -(\mathbf{m}_{sp}+\mathbf{T}^T\mathbf{m}_{pis}\mathbf{T})^{-1}\mathbf{k}_{sp} & -(\mathbf{m}_{sp}+\mathbf{T}^T\mathbf{m}_{pis}\mathbf{T})^{-1}(\mathbf{c}_{sp}+\mathbf{T}^T\mathbf{c}_{pis}\mathbf{T}) \\ -\mathbf{k}_{oil}\mathbf{k}_{v-c}\mathbf{k}_P\mathbf{T} & -\mathbf{k}_{oil}(\mathbf{k}_{v-c}\mathbf{k}_P\mathbf{k}_D\mathbf{T}+\mathbf{T}) \\ -\mathbf{T} & \mathbf{0} \end{bmatrix}$$

$$\begin{bmatrix} \mathbf{0} & \mathbf{0} \\ (\mathbf{m}_{sp}+\mathbf{T}^T\mathbf{m}_{pis}\mathbf{T})^{-1}\mathbf{T}^T & \mathbf{0} \\ \mathbf{k}_{oil}\mathbf{k}_{v-c}\mathbf{k}_P\mathbf{k}_{\Delta P}\mathbf{A}_{pis}^{-1}-\boldsymbol{\tau}_{lea}^{-1} & \mathbf{k}_{oil}\mathbf{k}_{v-c}\mathbf{k}_P\mathbf{k}_I^{-1} \\ \mathbf{0} & \mathbf{0} \end{bmatrix}$$

$$\mathbf{B}_{cs}=\begin{bmatrix} \mathbf{0} & \mathbf{0} \\ \mathbf{0} & \mathbf{0} \\ \mathbf{k}_{oil}\mathbf{k}_{v-c}\mathbf{k}_P\mathbf{T} & \mathbf{k}_{oil}\mathbf{k}_{v-c}\mathbf{k}_P(\mathbf{k}_D+\mathbf{k}_{FF})\mathbf{T} \\ \mathbf{T} & \mathbf{0} \end{bmatrix} \tag{79}$$

2.3.2 Formulation of the pseudo-dynamic testing set-up

Now, equation (53) will be rewritten as

$$\mathbf{r}_{sp}(t)=\mathbf{m}_{sp}\mathbf{a}_{sp}(t)+\mathbf{c}_{sp}\mathbf{v}_{sp}(t)+\mathbf{k}_{sp}\mathbf{d}_{sp}(t) \tag{80}$$

or having into account (61) and (66)

$$\begin{aligned}\mathbf{r}_{sp}(t)=\mathbf{m}_{sp}\left(\mathbf{m}_{sp}+\mathbf{T}^T\mathbf{m}_{pis}\mathbf{T}\right)^{-1}\left[\mathbf{T}^T\mathbf{F}_P(t)-\left(\mathbf{c}_{sp}+\mathbf{T}^T\mathbf{c}_{pis}\mathbf{T}\right)\mathbf{v}_{sp}(t)-\mathbf{k}_{sp}\mathbf{d}_{sp}(t)\right] \\ +\mathbf{c}_{sp}\mathbf{v}_{sp}(t)+\mathbf{k}_{sp}\mathbf{d}_{sp}(t)\end{aligned} \tag{81}$$

Thus, the N-DoF version of the PsD equation (45) is

$$\mathbf{m}_{PsD}\lambda^2\dot{\mathbf{v}}_{sp}^r(t)+\mathbf{c}_{PsD}\lambda\mathbf{v}_{sp}^r(t)+\mathbf{r}_{sp}(t)=\mathbf{f}_{INP}(t) \tag{82}$$

Where, again, the matrices of the theoretical mass $\mathbf{m}_{PsD}$ and viscous damping $\mathbf{c}_{PsD}$ of the specimen may differ from the physical ones $\mathbf{m}_{sp}$ and $\mathbf{c}_{sp}$.

Also, analogously to (41), for the case of seismic load, the vector of input forces to equation (82)

$$\mathbf{f}_{INP}(t)=-\mathbf{m}_{PsD}\mathbf{J}\mathbf{a}_g(t) \tag{83}$$

Where $\mathbf{a}_g$ is the vector of ground accelerograms and $\mathbf{J}$ is the matrix geometric influence for those accelerograms on the DoFs of the specimen.

A new expression will be obtained by solving $\dot{\mathbf{v}}_{sp}^r(t)$ from equation (82) and introducing (81)

$$\begin{aligned}\dot{\mathbf{v}}_{sp}^{r}(t) = \lambda^{-2}\mathbf{m}_{PsD}^{-1}\Big\{&\mathbf{f}_{INP}(t) - \mathbf{c}_{PsD}\lambda\mathbf{v}_{sp}^{r}(t) - \mathbf{m}_{sp}\left(\mathbf{m}_{sp} + \mathbf{T}^{T}\mathbf{m}_{pis}\mathbf{T}\right)^{-1}\mathbf{T}^{T}\mathbf{F}_{P} \\ &-\left[\mathbf{c}_{sp} - \mathbf{m}_{sp}\left(\mathbf{m}_{sp} + \mathbf{T}^{T}\mathbf{m}_{pis}\mathbf{T}\right)^{-1}\left(\mathbf{c}_{sp} + \mathbf{T}^{T}\mathbf{c}_{pis}\mathbf{T}\right)\right]\mathbf{v}_{sp}(t) \\ &-\left[\mathbf{I} - \mathbf{m}_{sp}\left(\mathbf{m}_{sp} + \mathbf{T}^{T}\mathbf{m}_{pis}\mathbf{T}\right)^{-1}\right]\mathbf{k}_{sp}\mathbf{d}_{sp}(t)\Big\}\end{aligned} \tag{84}$$

Now, the state equation for the N-DoF PsD test is written as

$$\dot{\mathbf{x}}(t) = \mathbf{A}\mathbf{x}(t) + \mathbf{B}\mathbf{u}(t) \tag{85}$$

where, by choice,

$$\mathbf{x}(t) = \begin{bmatrix} \mathbf{d}_{sp}^{r}(t) \\ \mathbf{v}_{sp}^{r}(t) \\ \mathbf{d}_{sp}(t) \\ \mathbf{v}_{sp}(t) \\ \mathbf{F}_{P}(t) \\ \boldsymbol{\varepsilon}_{I}(t) \end{bmatrix} \quad ; \quad \mathbf{u}(t) = \left[\mathbf{f}_{INP}(t)\right] \tag{86}$$

are the state and input vectors respectively.

In this case, the coefficients of the matrices in (85) are derived in row-order from expressions (57), (84), (60), (66), (74) and (72) as

$$\mathbf{A} = \begin{bmatrix} \mathbf{0} & \mathbf{I} \\ \mathbf{0} & -\lambda^{-1}\mathbf{m}_{PsD}^{-1}\mathbf{c}_{PsD} \\ \mathbf{0} & \mathbf{0} \\ \mathbf{0} & \mathbf{0} \\ \mathbf{k}_{oil}\mathbf{k}_{v-c}\mathbf{k}_{P}\mathbf{T} & \mathbf{k}_{oil}\mathbf{k}_{v-c}\mathbf{k}_{P}(\mathbf{k}_{D} + \mathbf{k}_{FF})\mathbf{T} \\ \mathbf{T} & \mathbf{0} \end{bmatrix}$$

$$\begin{bmatrix} \mathbf{0} & \mathbf{0} \\ -\lambda^{-2}\mathbf{m}_{PsD}^{-1}\mathbf{T}^{T}\mathbf{m}_{pis}\mathbf{T}(\mathbf{m}_{sp} + \mathbf{T}^{T}\mathbf{m}_{pis}\mathbf{T})^{-1}\mathbf{k}_{sp} & \lambda^{-2}\mathbf{m}_{PsD}^{-1}\left[\mathbf{m}_{sp}(\mathbf{m}_{sp} + \mathbf{T}^{T}\mathbf{m}_{pis}\mathbf{T})^{-1}(\mathbf{c}_{sp} + \mathbf{T}^{T}\mathbf{c}_{pis}\mathbf{T}) - \mathbf{c}_{sp}\right] \\ \mathbf{0} & \mathbf{I} \\ -(\mathbf{m}_{sp} + \mathbf{T}^{T}\mathbf{m}_{pis}\mathbf{T})^{-1}\mathbf{k}_{sp} & -(\mathbf{m}_{sp} + \mathbf{T}^{T}\mathbf{m}_{pis}\mathbf{T})^{-1}(\mathbf{c}_{sp} + \mathbf{T}^{T}\mathbf{c}_{pis}\mathbf{T}) \\ -\mathbf{k}_{oil}\mathbf{k}_{v-c}\mathbf{k}_{P}\mathbf{T} & -\mathbf{k}_{oil}(\mathbf{k}_{v-c}\mathbf{k}_{P}\mathbf{k}_{D}\mathbf{T} + \mathbf{T}) \\ -\mathbf{T} & \mathbf{0} \end{bmatrix}$$

$$\begin{bmatrix} \mathbf{0} & \mathbf{0} \\ -\lambda^{-2}\mathbf{m}_{PsD}^{-1}\mathbf{m}_{sp}(\mathbf{m}_{sp}+\mathbf{T}^T\mathbf{m}_{pis}\mathbf{T})^{-1}\mathbf{T}^T & \mathbf{0} \\ \mathbf{0} & \mathbf{0} \\ (\mathbf{m}_{sp}+\mathbf{T}^T\mathbf{m}_{pis}\mathbf{T})^{-1}\mathbf{T}^T & \mathbf{0} \\ \mathbf{k}_{oil}\mathbf{k}_{v-c}\mathbf{k}_P\mathbf{k}_{\Delta P}\mathbf{A}_{pis}^{-1}-\boldsymbol{\tau}_{lea}^{-1} & \mathbf{k}_{oil}\mathbf{k}_{v-c}\mathbf{k}_P\mathbf{k}_I^{-1} \\ \mathbf{0} & \mathbf{0} \end{bmatrix}$$

$$\mathbf{B}=\begin{bmatrix} \mathbf{0} \\ \lambda^{-2}\mathbf{m}_{PsD}^{-1} \\ \mathbf{0} \\ \mathbf{0} \\ \mathbf{0} \\ \mathbf{0} \end{bmatrix} \tag{87}$$

3 EXPERIMENTAL SET-UP

For the calibration of the developed analytical model for a particular example, we chose a 1-DoF steel specimen controlled by two actuators (***Figure 2***) and tested at ELSA by using the ELSA testing system. The experimental set-up for this example is described in this chapter, while the comparison of experimental and analytical results is done afterwards.

3.1 Specimen

The specimen consisted of a one-bay-by-one-bay steel frame with one storey that had been used before for NEFOREEE project (Bairrao et al., 2004). The beams were positioned at a height of 3 m and the distance between columns in the direction of the excitation (X axis) was also 3 m. The columns were made of HEB 100 profiles while the beams had HEB 180 sections. The steel grade was S355. Columns and beams were bolted to the steel joints. For the placement of the upper slab, 8 tons of concrete were poured in situ. The total weight of the specimen was around 10 tons.

3.2 Testing devices

For the execution of the PsD tests at the ELSA reaction wall, the specimen was clamped onto the strong horizontal floor. The PsD loading set-up consisted of two 200 kN MOOG hydraulic actuators acting symmetrically in the horizontal longitudinal direction, with one end fixed to the concrete slab of the model and the other one to the vertical reaction wall. The servo-valves used at these actuators had a capacity of 38 litre/min each.

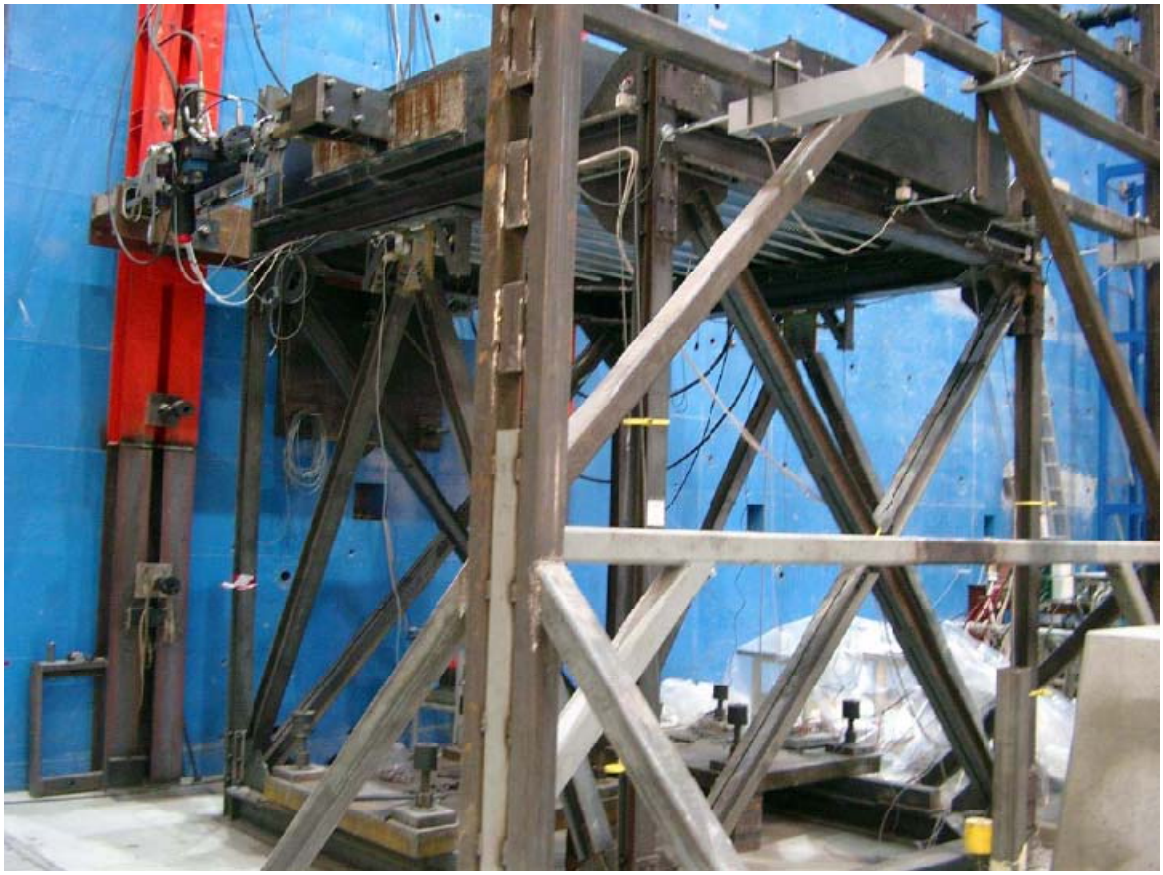

Figure 2. NEFOREEE 1-DoF steel frame at ELSA laboratory.

For the PsD tests, the relative displacements of the slab to the base was measured by two HEIDENHAIN optical encoder displacement transducers fixed on a reference frame and used for the control of both actuators. However, for the dynamic characterising test of the control system that is described in the following section, two analogue (potencimeter) displacement transducers, set in parallel with the HEIDENHAIN transducers, were used as feedback.

4 FREQUENCY RESPONSE CHARACTERISING TEST OF THE CONTROL SYSTEM

In order to characterise experimentally the control system for our testing set-up for the NEFOREEE specimen, a sine chirp test was performed with the same reference signal for both actuators. The sine chirp test is one of the excitation techniques used for identification of Frequency Response Functions (FRFs). Because of its deterministic character as a test, it is especially used with systems that are almost linear (Avitabile, 2005).

4.1 Sine chirp test

In a sine chirp test the excitation signal contains a sine swept that is repeated periodically, so that, if the acquisition is done after the response is stabilised and the analysis of the FRFs is performed taking whole periods of the signals, there are no leakage errors.

The sine swept was prepared in a file containing a signal with a sampling period of 2ms and $2^{19} = 524288$ points (duration of 1048.576 s) with a sinus signal that swept the frequency logarithmically from 0.02 Hz to 15 Hz with variable amplitude. For

frequencies between 0.02 and 0.1 Hz, the amplitude of the signal had the nominal value of 10 mm. Between 0.1 and 2.0 Hz, the amplitude was gradually reduced from 10 to 1mm. And, for frequencies between 2.0 and 15 Hz, the amplitude was kept constant at 1mm (***Figure 3***). This progressive reduction of the amplitudes for increasing frequencies was necessary in order to avoid excessive displacement around the resonance of the control system, as well as avoiding excessive velocity at the displacement transducers. Since this reference signal was going to be introduced in a periodic manner, in order to avoid the jump from the final value to the initial zero, the amplitude of the last 100 points was also modulated to gradually decrease up to zero. The obtained time history of the reference signal is plotted in ***Figure 4***. In order to produce tests with different amplitudes, this reference signal was multiplied by a span factor before it was sent to the controller.

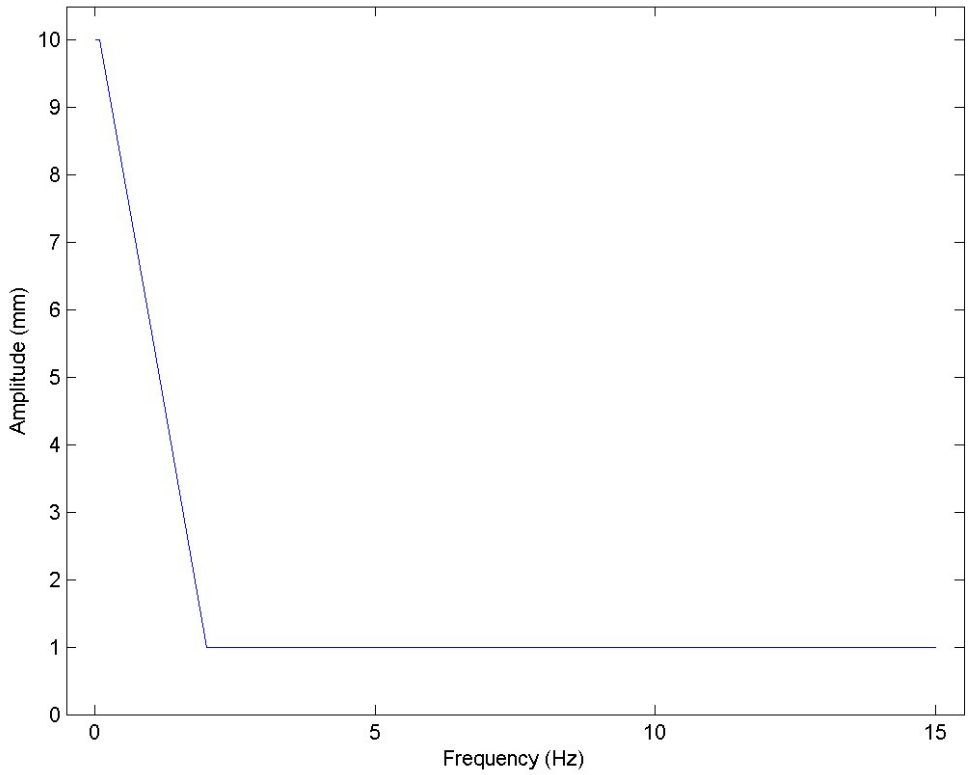

Figure 3. Reference signal for the sine chirp test. Variation of amplitude with respect to frequency.

Even though the sampling period of the acquisition was originally 2ms as for the reference signal, the saved measurements at the acquisition were based on an average value of 8 consecutive sampled values of 2ms. Thus, the obtained saved values of the acquisition had a sampling period of 16ms. The treatment of the acquisition signals used 65536 points with sampling period of 16 ms that corresponded exactly to one period of the reference signal (1048.576 s).

4.2 Test results

The results of different runs of this sine chirp test will be shown in this subsection. As displayed in Table 1, the reference displacement amplitude, as well as the proportional and integral gains of the controllers, had different values at the different runs in order to experimentally assess their effect on the results.

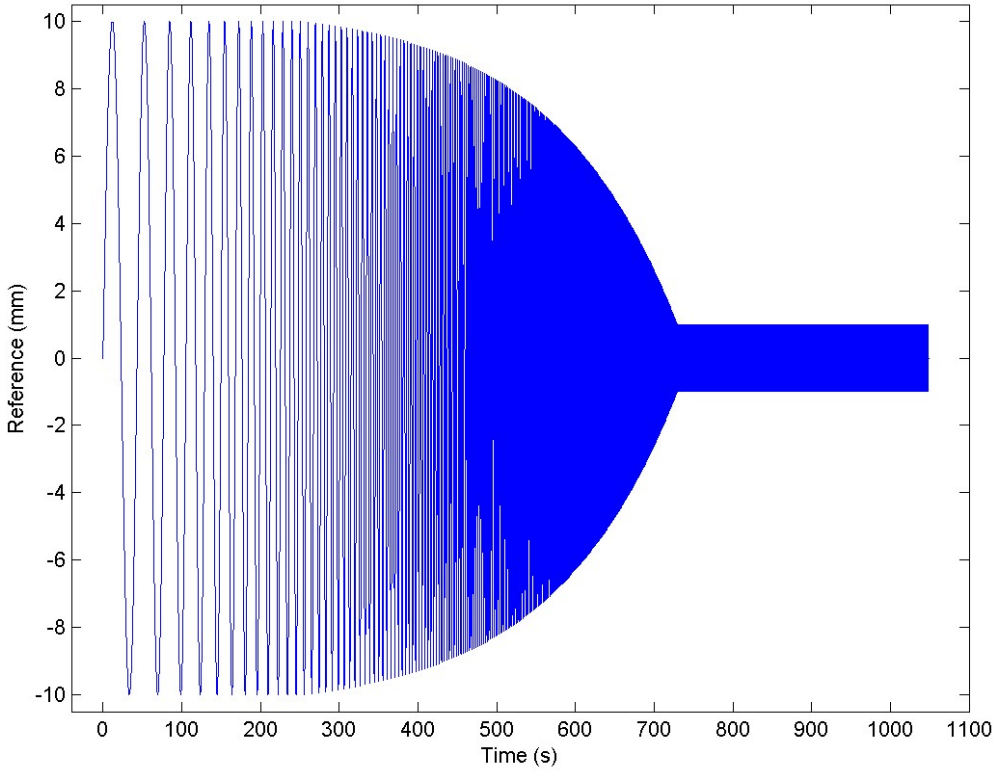

Figure 4. Reference signal for the sine chirp test. Time history.

Table 1. Different runs of sine chirp test "n53".

Test run	Reference amplitude (mm)	P_{scr} proportional gain (at controllers screen)	I_{scr} integral gain (at controllers screen)
7	6	0.1	500
8	6	0.2	500
10	6	0.2	200
11	6	0.2	50
12	3	0.2	500
13	1	0.2	500
14	6	0.5	500
15	6	0.1	500
16	6	0.2	500

The test was run in a continuous manner, changing the parameters from the values of one run to the successive one without stopping. The reference signal was periodic and the acquisition was done at least 500 s after the start of any of the runs in order to let the system stabilise. Then, by taking exactly one period of the response, the FFT could be applied with a uniform window and without any leakage. In order to diminish the effects of the noise on the FRFs, the FFT-obtained cross (or power) spectral density functions were smoothed by convolving them by a Hanning window of 31 points that corresponds to a band width of

$$\Delta f = \left(\frac{1}{2}\right)\frac{31}{1048.576} = 0.015 \text{ Hz} \tag{88}$$

which can roughly be considered as the resolution of the obtained spectra, at least in the areas with a coherence value close to 1 (Ewins, 1984).

Figure 5 to ***Figure 10*** correspond to results of runs 11, 10 and 16 in Table 1, for which the nominal amplitude was 6 mm and the P parameter was 0.2, while the I parameter changed from run to run. ***Figure 5*** shows the acquired reference signals which were identical at the controllers of both actuators. The acquisitions for the different runs, do not start at the beginning of the sine swept, but they cover exactly one period of the excitation as already commented. ***Figure 6*** shows the time history of the analogue displacements measured at the top slab of the specimen and used for the feedback of the respective controllers. Unfortunately, at run 11, with I=50, there was a saturation of the analogue displacement transducers around a resonance frequency of the control. This saturation cuts the response for frequencies between 0.9 and 1.0 Hz and the effects will be seen in the spectra. This saturation of the measurements did not happen for any other run of the test. The average value of the two displacements was then used for computing the FRFs shown in the three graphs of ***Figure 7*** that correspond to amplitude, phase and coherence. As we will see in general for most of the runs, the coherence was excellent for frequencies lower than 1.5 Hz and then, for higher frequencies, depending on how large the response was in that area, the coherence was still acceptable or not good any more. As announced, the mentioned saturation at run 11, is seen in the blue curves (for I=50) sometimes for frequencies between 0.9 and 1.0 Hz and at their multiples. As seen in the comparison of these curves, the interest in using low values of the I parameter in PsD tests is because the phase lag between reference signal and measured displacement is kept almost null for a wider range of frequencies. The negative effect of this is an amplification of the peak of resonance in the control system and also the risk of instability. ***Figure 8*** shows also the estimation of the open-loop FRF of the controller obtained as the relationship between the error signal (reference minus analogue displacement) and the analogue displacement. Please note that this open-loop FRF estimation was done from the results of the closed-loop control configuration test. In fact, the coherence for this FRF is not good at low frequencies because the error there was too small in comparison to the noise of the signals. ***Figure 9*** shows the FRF between the analogue displacement and the HEIDENHAIN digital transducer and ***Figure 10*** shows the FRF between the analogue displacement and the TEMPOSONICS digital transducer. Apart from the effects of the saturation, also seen here for the blue curve, we can observe how the measures of the HEIDENHAIN and the TEMPOSONICS start to lose quality in amplitude and phase for frequencies greater than 2 Hz. Because of this limitation, the analogue displacement was chosen as feedback for this dynamic test with reduced amplitude. Those HEIDENHAIN and TEMPOSONICS transducers are convenient for

PsD quasistatic tests because they give high resolution and large displacement range at the same time. However, they cannot be used for dynamic tests as shown here.

Figure 11 to ***Figure 15*** correspond to results of runs 16, 12 and 13 in Table 1, for which the I parameter was 500 and the P parameter was 0.2, while the nominal amplitude changed from run to run. ***Figure 11*** shows the time history of the analogue displacements without saturation for these runs. Again, the average value of the two displacements was then used for computing the FRFs. The closed-loop and open-loop FRFs of the control system are shown in ***Figure 12*** and ***Figure 13***, where the coherences are good between 0.02 and 1.5 Hz, but deteriorate for higher frequencies, especially for the smallest amplitude run. The comparison of the three FRFs for these three runs in the area of good coherence can be considered as a check of linearity of the control system within these values of amplitude and in fact it shows a good linearity because the three FRF are almost equal. ***Figure 14*** and ***Figure 15*** show the FRFs between the analogue displacement and the digital transducers. Again, we can observe how the measures of the HEIDENHAIN and the TEMPOSONICS start to lose quality in amplitude and phase for frequencies greater than 2 Hz. Apparently, the quality of the measurement for these digital transducers is lost for those frequencies independently of the amplitude, at least for the studied range.

Finally, ***Figure 16*** to ***Figure 19*** correspond to results of runs 14, 16, 15, 8 and 7 in Table 1, for which the nominal amplitude was 6 mm and the I parameter was 500, while the P parameter changed from run to run. The closed-loop and open-loop FRFs of the control system are shown in ***Figure 16*** and ***Figure 17***, where the runs that had equal parameter setting also show almost equal FRF. As seen in the comparison of these curves, the interest in using high values of the P parameter in PsD tests is because the gain and the phase lag between reference signal and measured displacement is kept good for a wider range of frequencies. As for the I parameter, the negative effect of this is an amplification of the peak of resonance in the control system and also the risk of instability. Also in this occasion, from ***Figure 18*** and ***Figure 19***, we can observe how the measures of the HEIDENHAIN and the TEMPOSONICS start to lose quality in amplitude and phase for frequencies greater than 2 Hz.

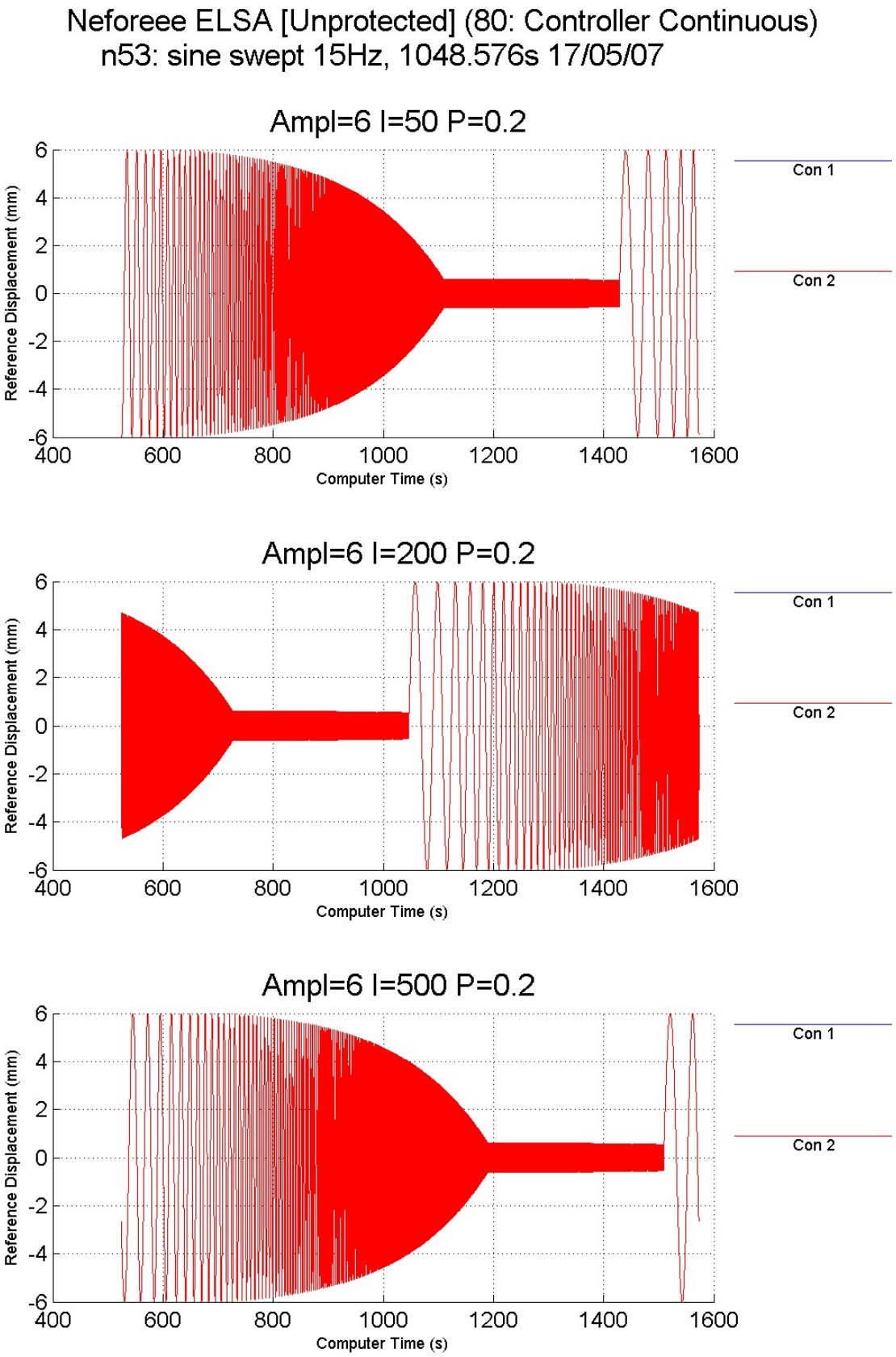

Figure 5. Sine chirp test. Time histories of reference signal for varying I parameter.

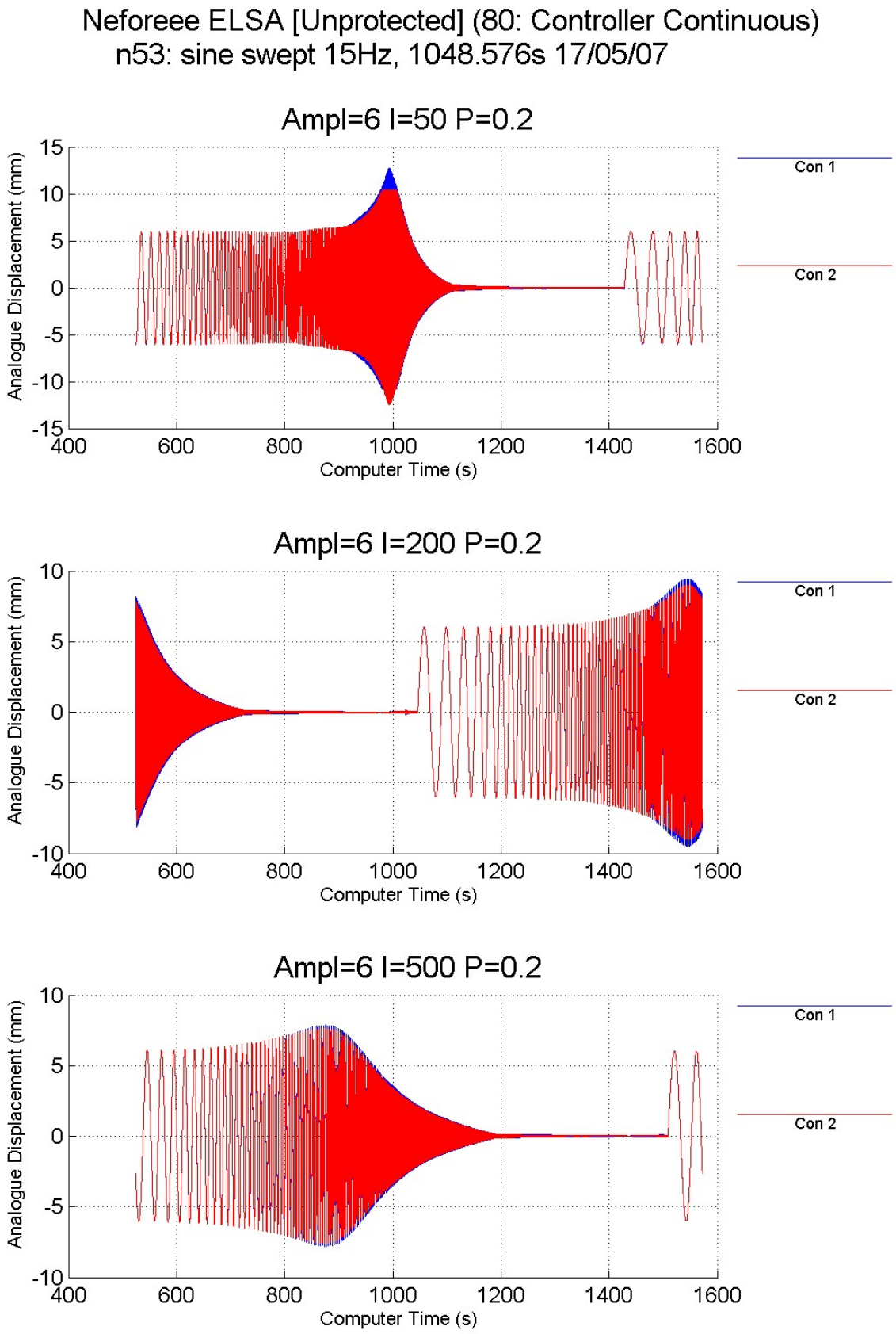

Figure 6. Sine chirp test. Time histories of measured displacement for varying I parameter.

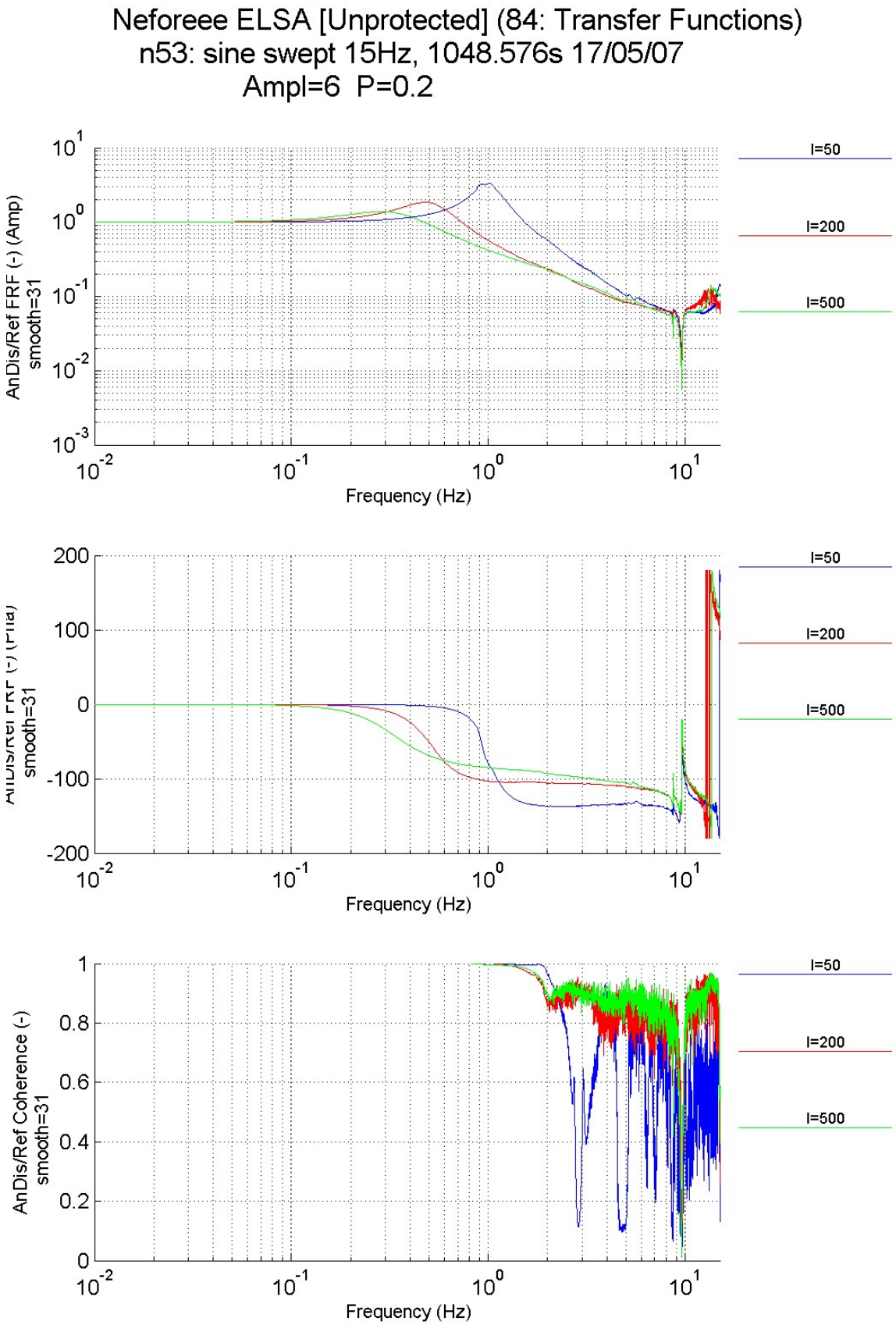

Figure 7. Sine chirp test. Closed-loop FRFs for varying I parameter.

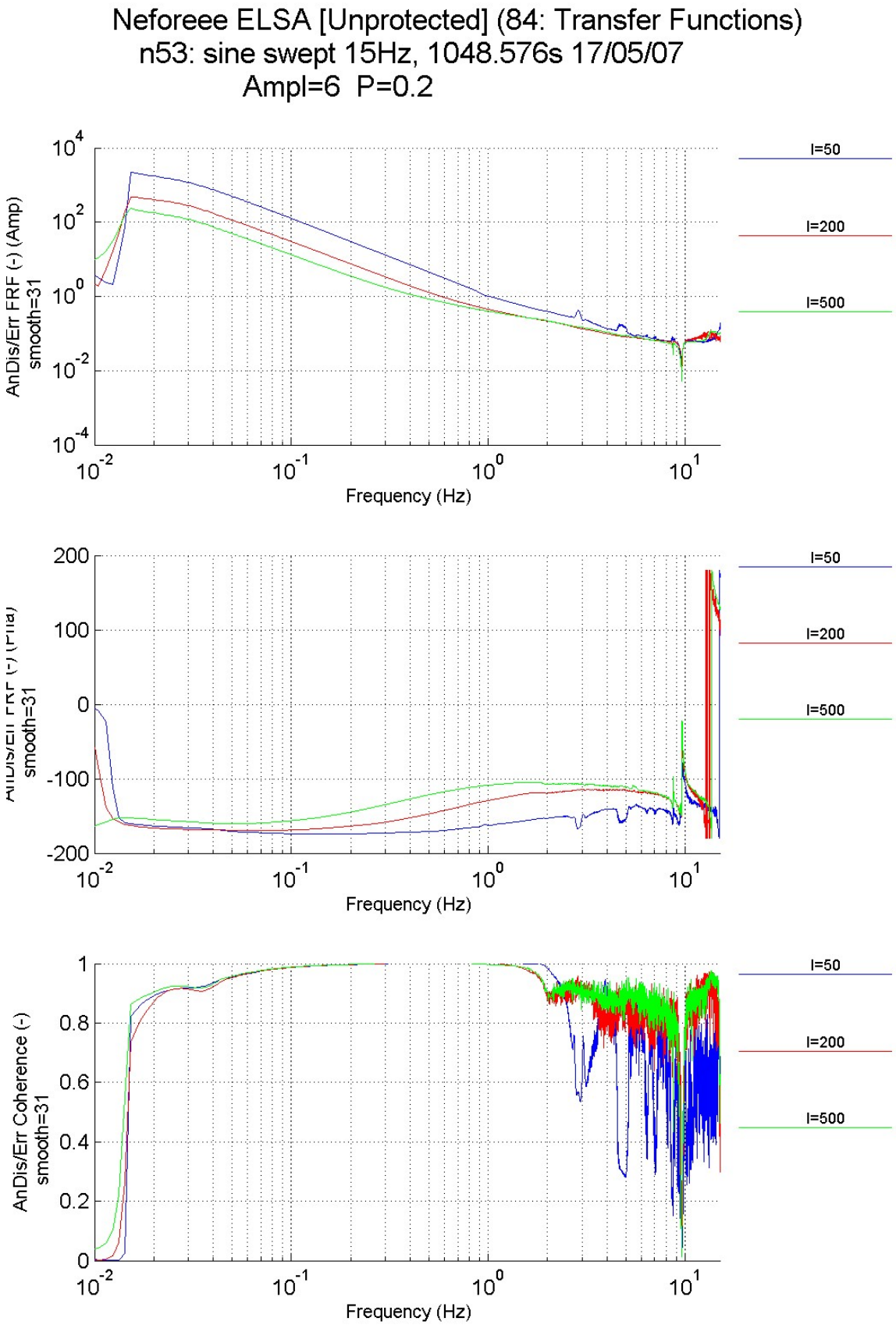

Figure 8. Sine chirp test. Open-loop FRFs for varying I parameter.

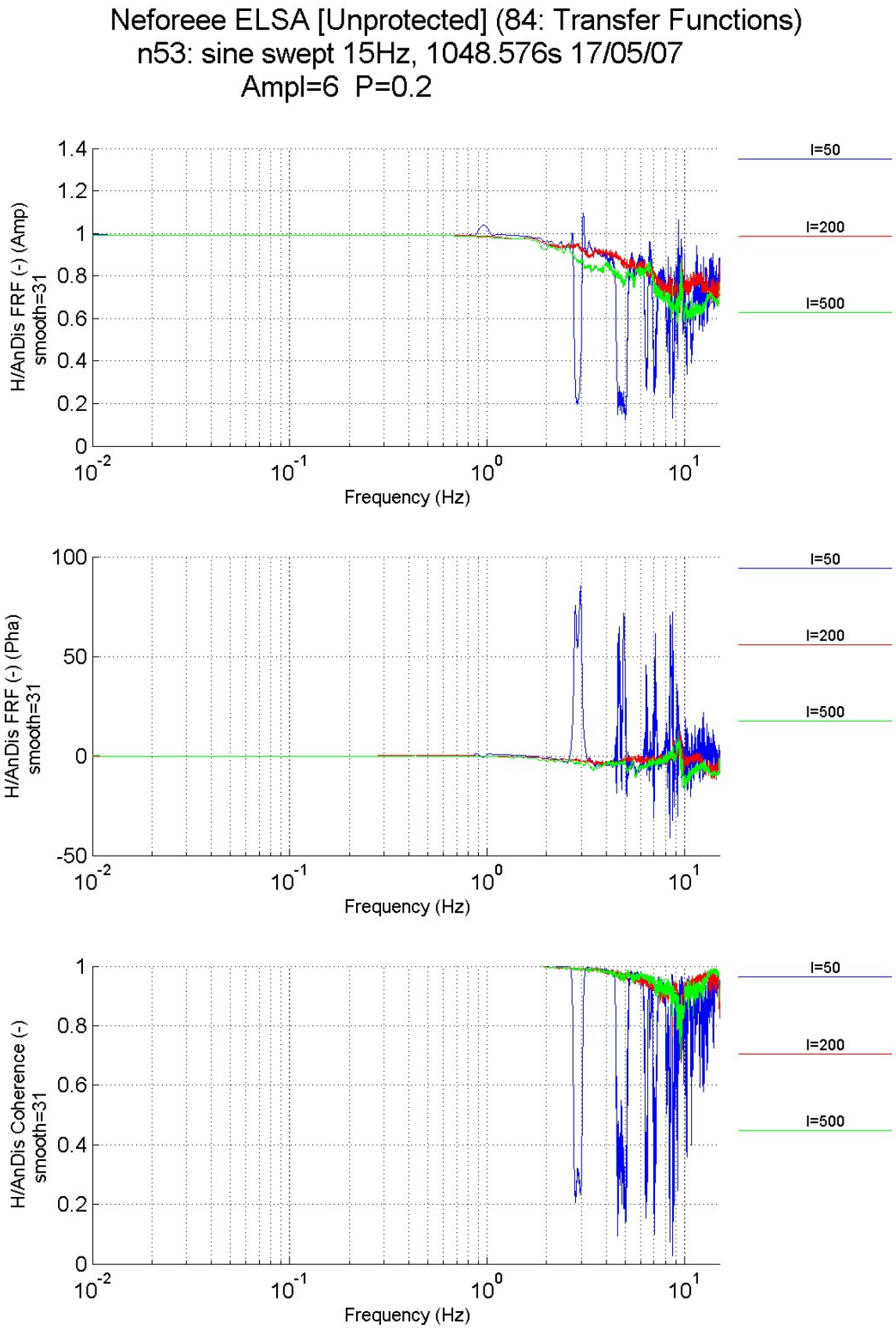

Figure 9. Sine chirp test. FRFs between analogue and Heidenhain displacements for varying I parameter.

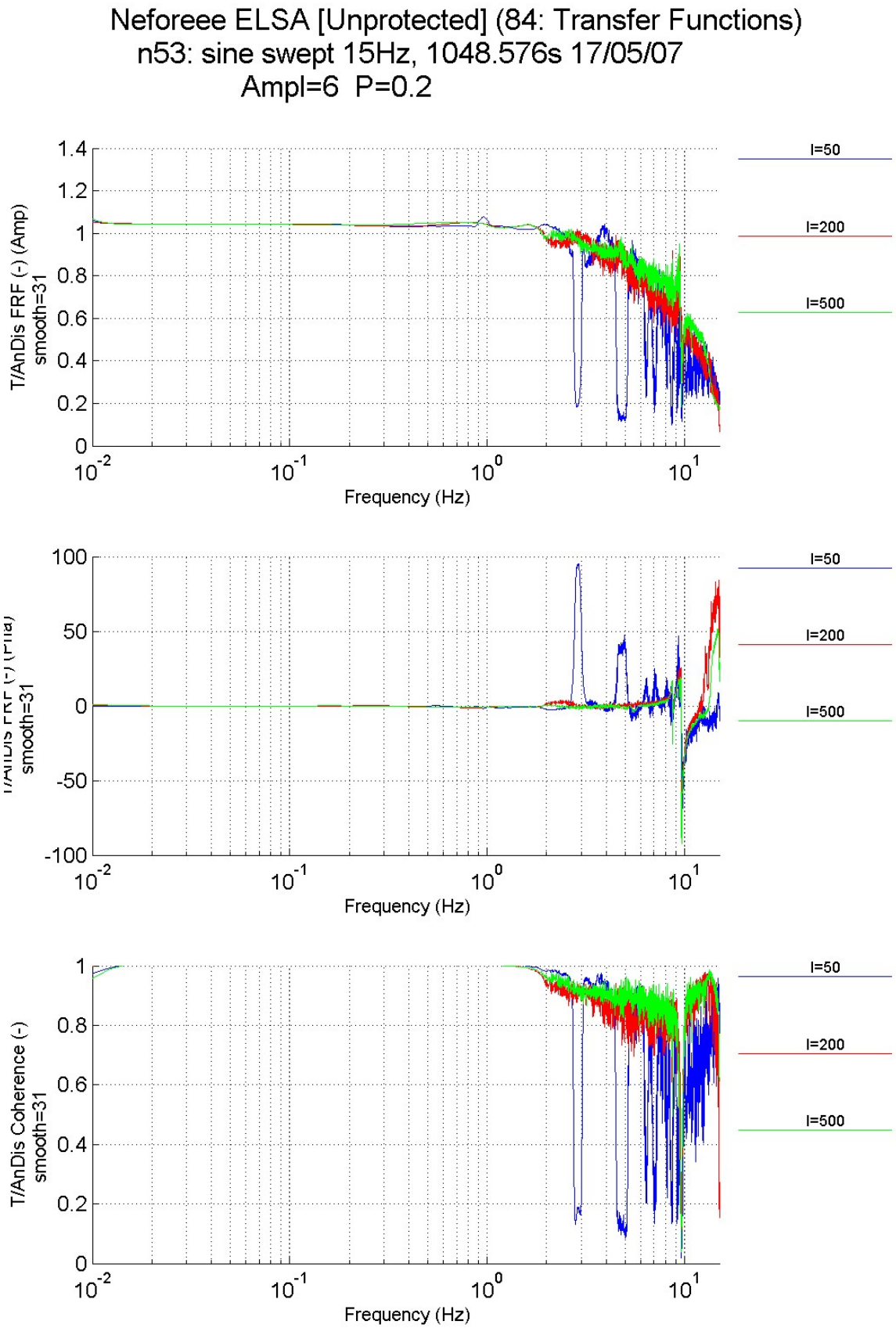

Figure 10. Sine chirp test. FRFs between analogue and Temposonics displacements for varying I parameter.

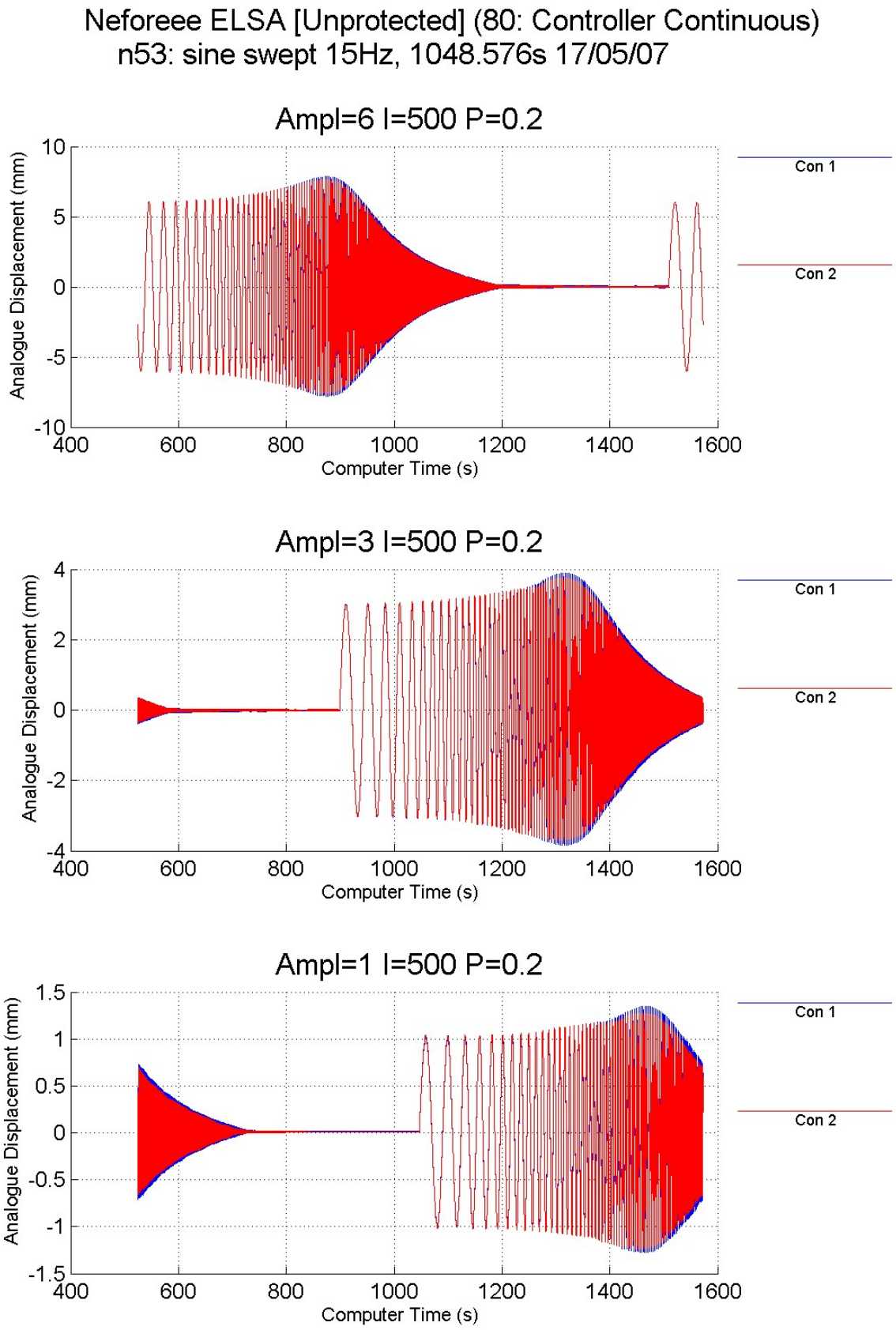

Figure 11. Sine chirp test. Time histories of measured displacement for varying amplitude.

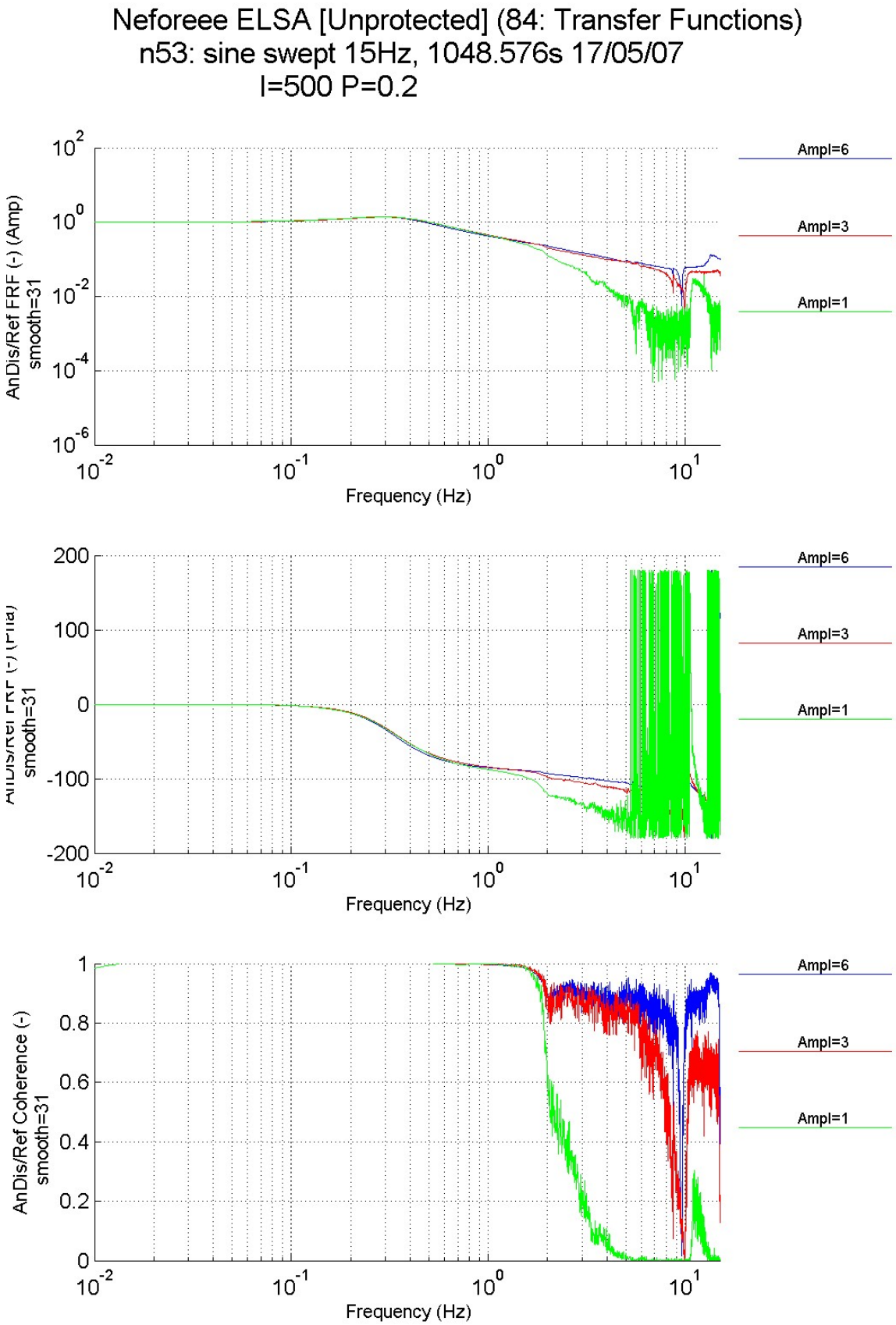

Figure 12. Sine chirp test. Closed-loop FRFs for varying amplitude.

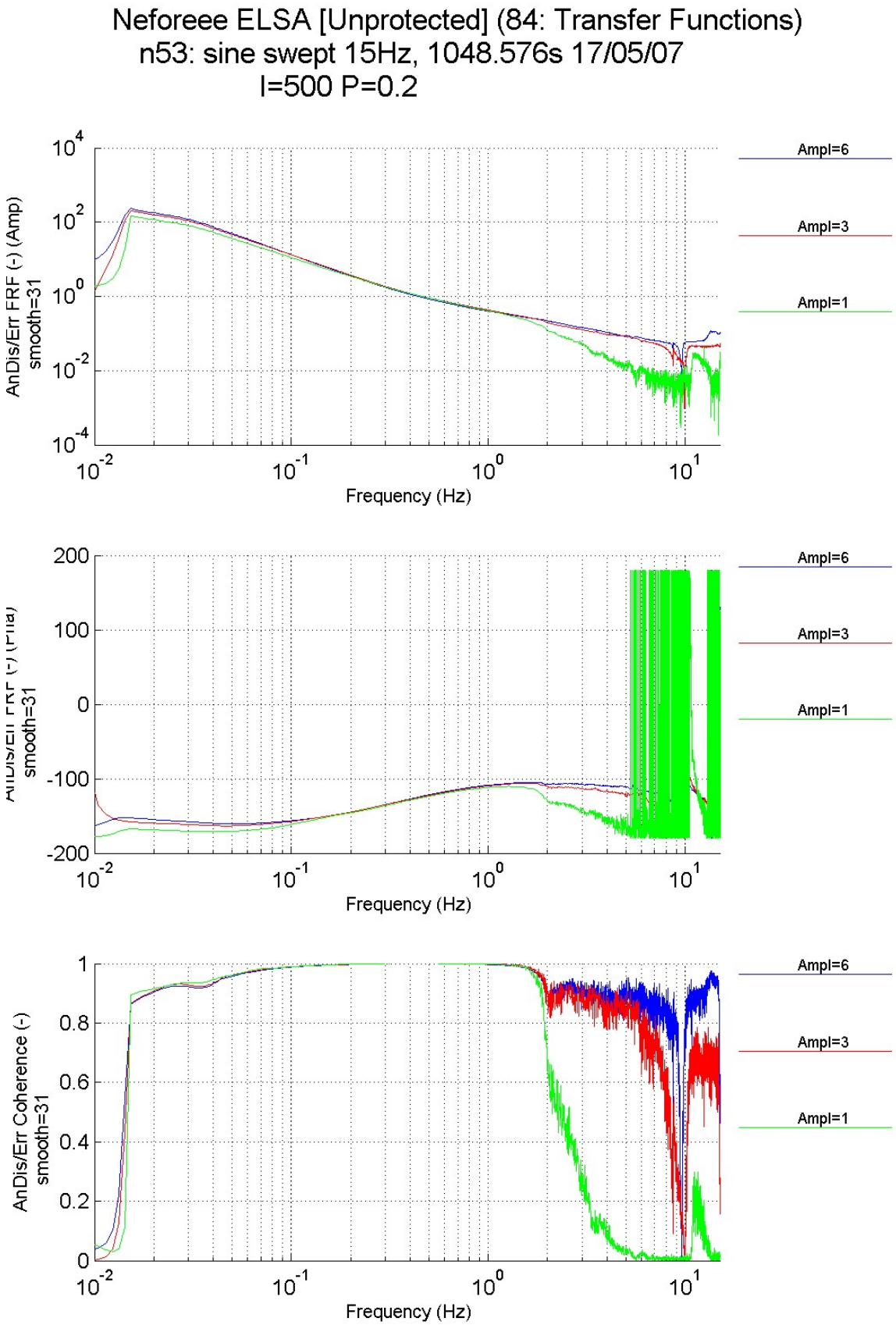

Figure 13. Sine chirp test. Open-loop FRFs for varying amplitude.

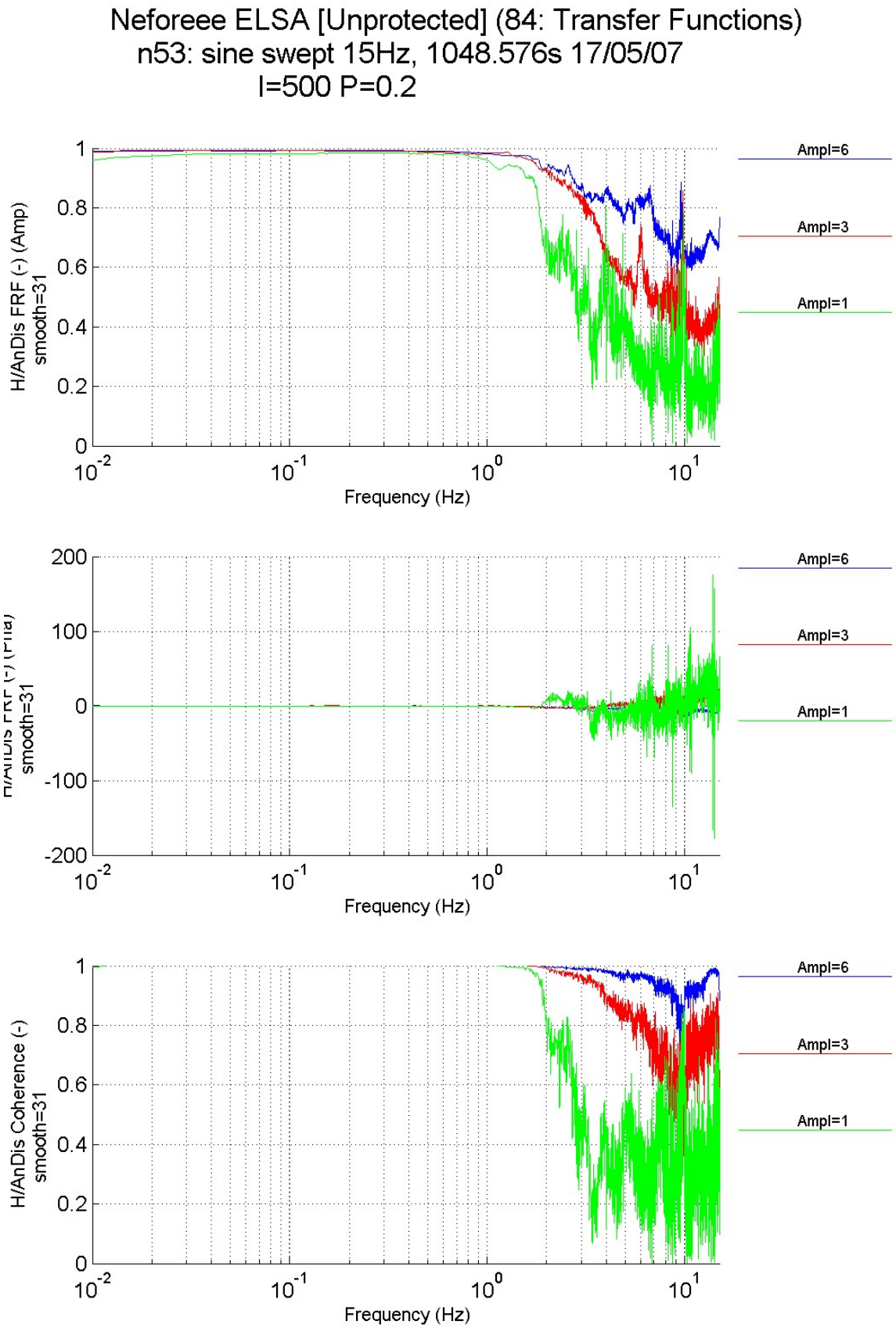

Figure 14. Sine chirp test. FRFs between analogue and Heidenhain displacements for varying amplitude.

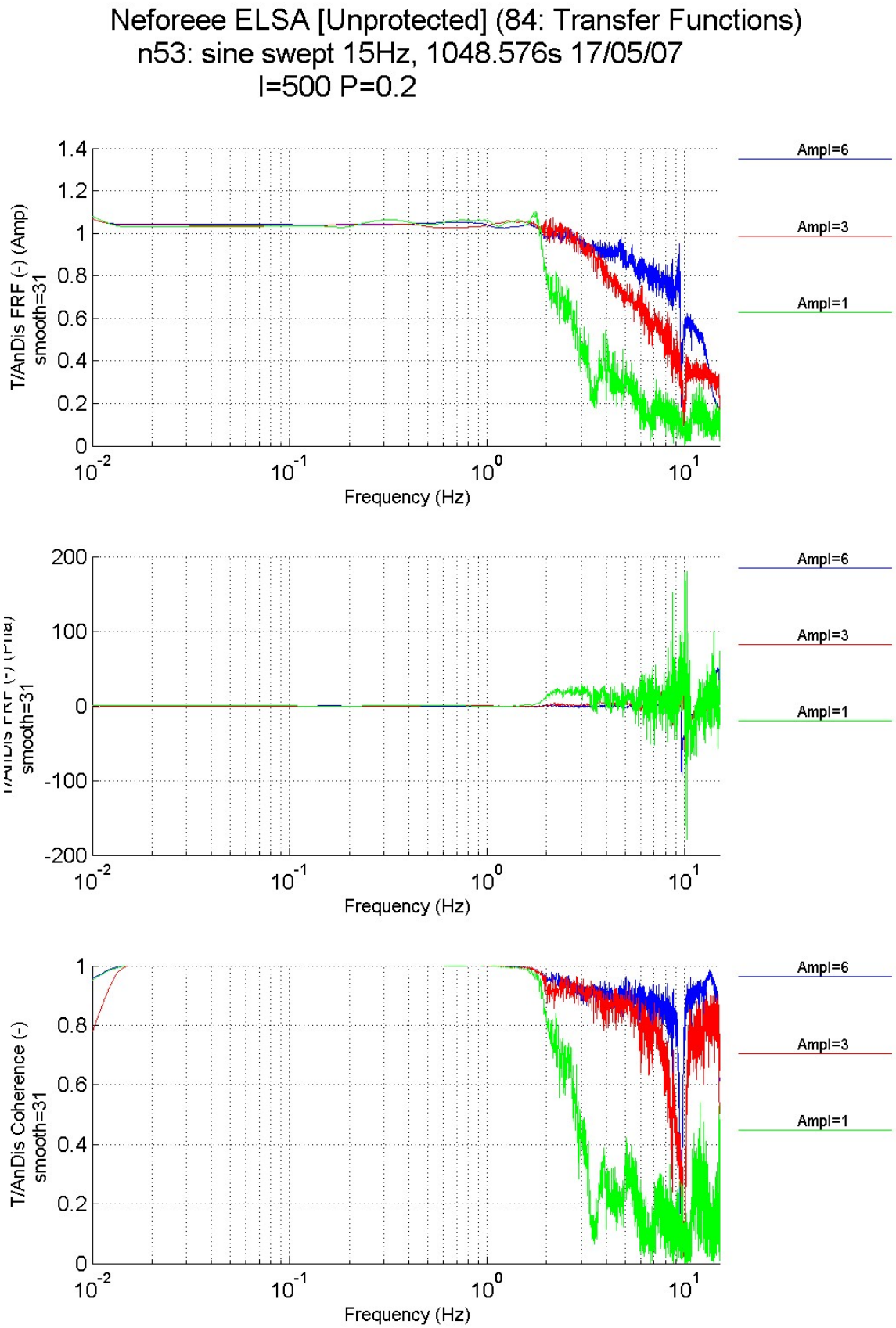

Figure 15. Sine chirp test. FRFs between analogue and Temposonics displacements for varying amplitude.

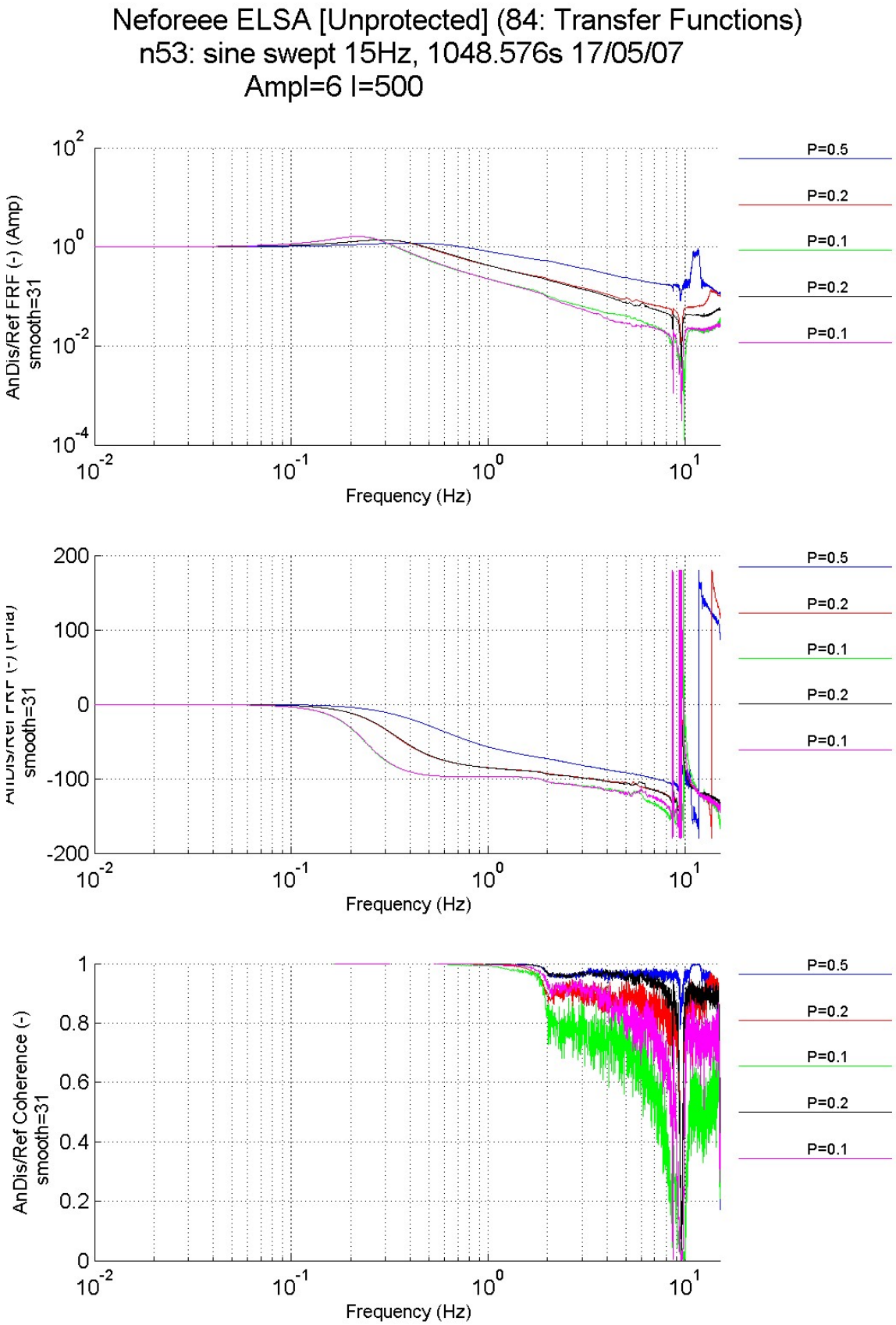

Figure 16. Sine chirp test. Closed-loop FRFs for varying P parameter.

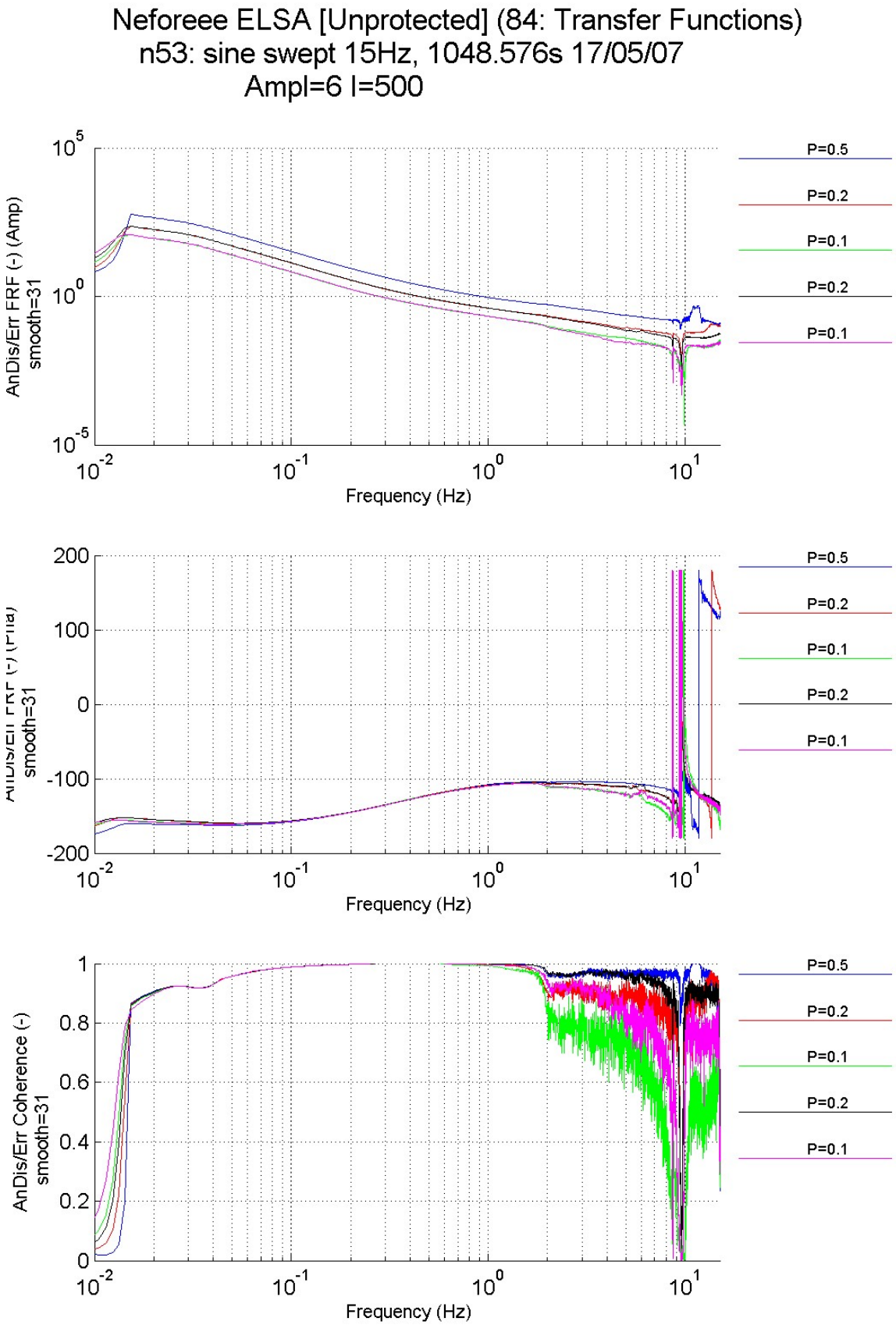

Figure 17. Sine chirp test. Open-loop FRFs for varying P parameter.

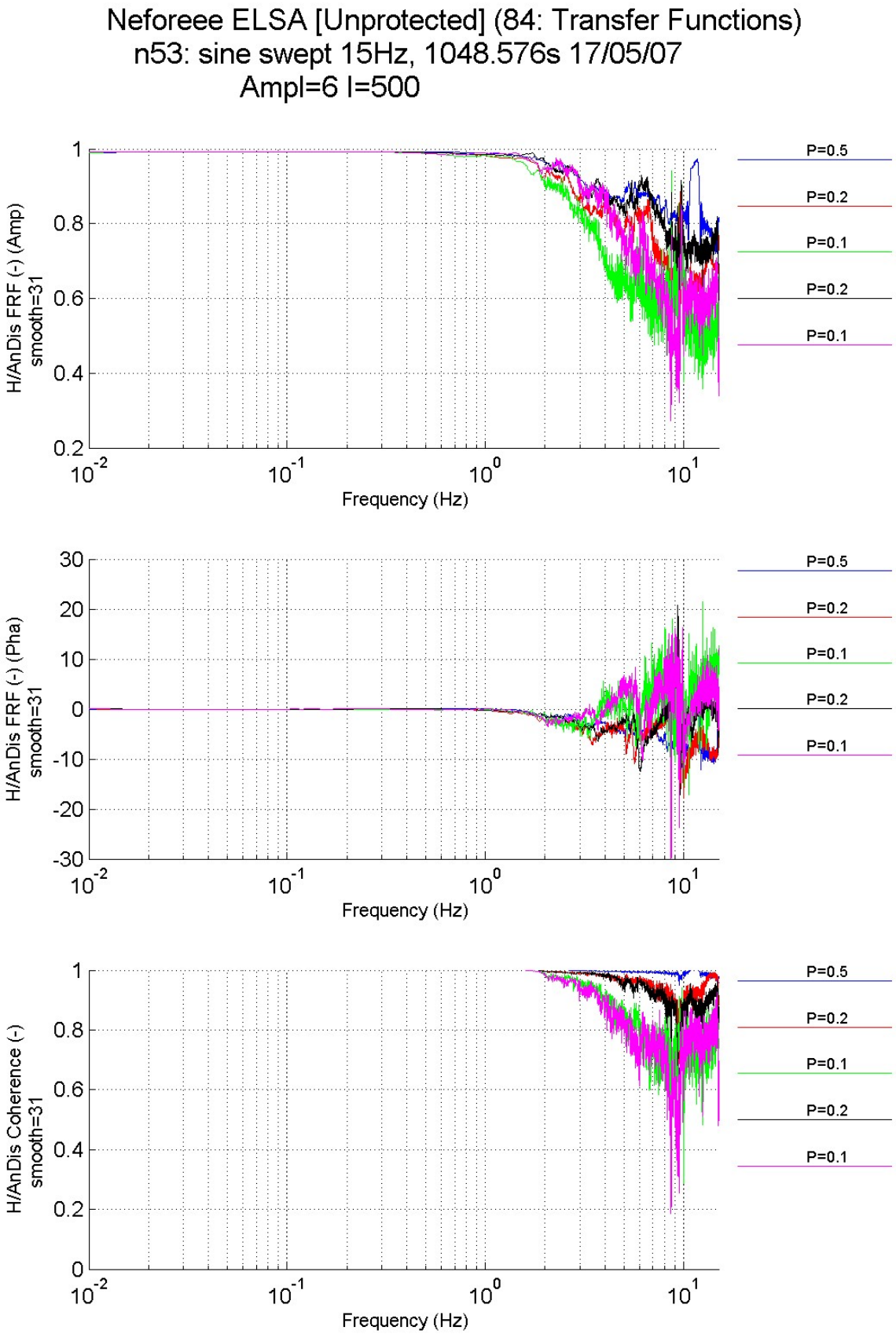

Figure 18. Sine chirp test. FRFs between analogue and Heidenhain displacements for varying P parameter.

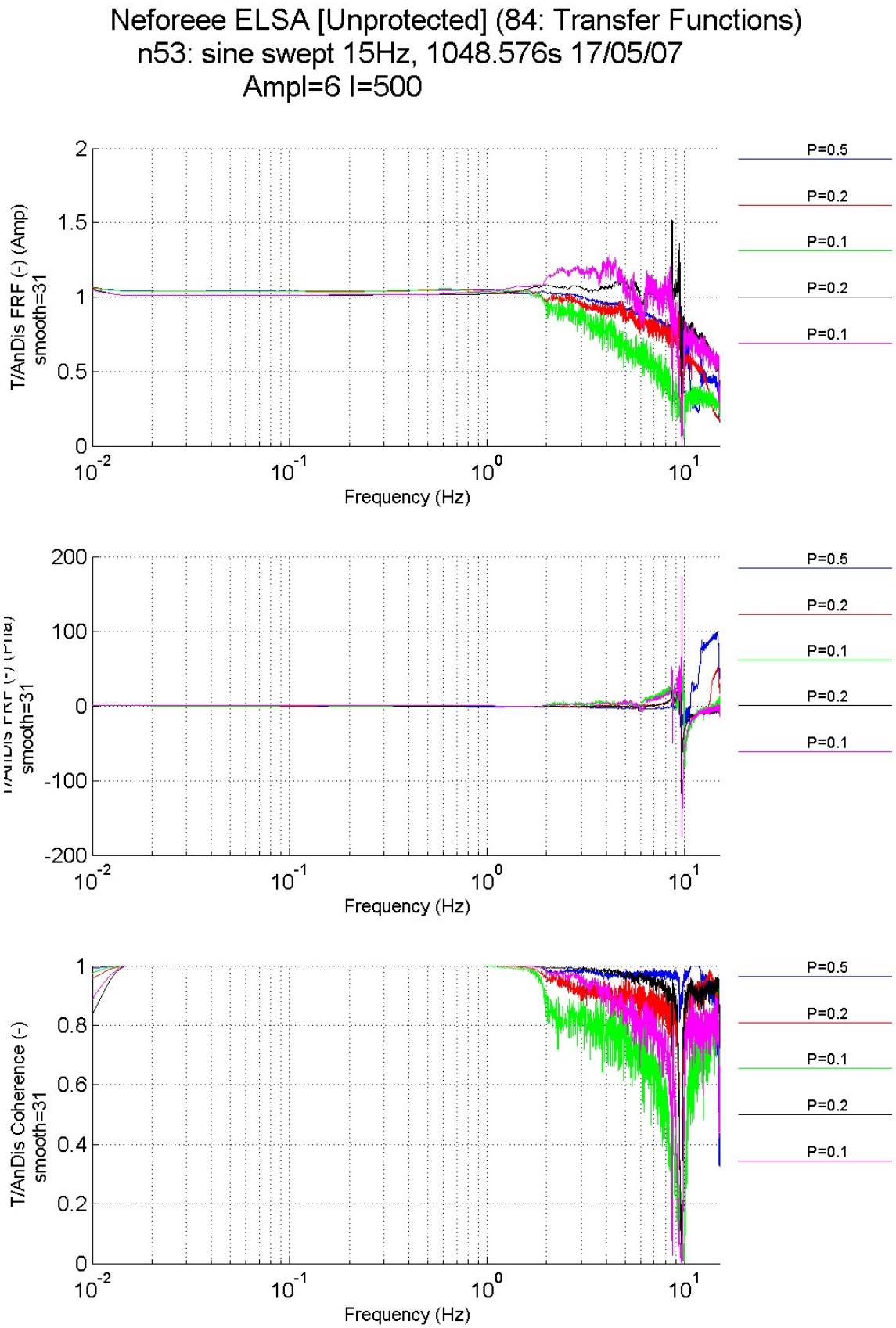

Figure 19. Sine chirp test. FRFs between analogue and Temposonics displacements for varying P parameter.

4.3 Calibration of the analytical model

The analytical linear model developed in section 2 was applied to the experimental set-up and tests described in sections 3 and 4 in order to calibrate the model by comparison with the experimental results.

4.3.1 Analytical parameters determined before the experiment

The parameters of the analytical model covered in this subsection were determined from the geometry or characteristics of the devices as well as from dynamic measurements on the specimen that were available before the test.

Regarding the specimen, considering it as a 1-DoF system, all the characteristics were known from previous tests done for the NEFOREEE project (Molina et al., 2008). Thus, the mass was assigned

$$m_{sp} = 8000 \quad kg \tag{89}$$

the stiffness

$$k_{sp} = 2.135 \cdot 10^6 \quad N/m \tag{90}$$

and the equivalent viscous damping

$$c_{sp} = 2.614 \cdot 10^3 \quad Ns/m \tag{91}$$

which corresponded to an eigenfrequency of 2.6 Hz and a damping ratio of 0.01.

Regarding the two actuators, by knowing their geometry and material density, the mass matrix of the pistons was

$$\mathbf{m}_{pis} = \begin{bmatrix} 67.5 & 0 \\ 0 & 67.5 \end{bmatrix} \quad kg \tag{92}$$

and the matrix of piston sections was

$$\mathbf{A}_{pis} = \begin{bmatrix} 0.010367 & 0 \\ 0 & 0.010367 \end{bmatrix} \quad m^2 \tag{93}$$

For the parameters of the controller algorithm for this test, we had for the proportional gain

$$\mathbf{k}_P = 1000 \begin{bmatrix} P_{scr} & 0 \\ 0 & P_{scr} \end{bmatrix} \quad m^{-1} \tag{94}$$

and for the integral gain

$$\mathbf{k}_I = 0.001 \begin{bmatrix} I_{scr} & 0 \\ 0 & I_{scr} \end{bmatrix} \quad s \tag{95}$$

where P_{scr} and I_{scr} are the value of these parameters shown in the screen of the controller and specified in Table 1 for every run of the test. All the other gains were null

$$\mathbf{k}_D = \mathbf{k}_{FF} = \mathbf{k}_{\Delta P} = \begin{bmatrix} 0 & 0 \\ 0 & 0 \end{bmatrix} \tag{96}$$

Note that the feed-forward and differential pressure gains are not currently programmed in our controller algorithm, while the differential term we use to keep null for this type of control system. All these gain matrices are diagonal because the control algorithm runs independently for every actuator in our case.

The servo-valves had a nominal capacity of 38 l/min for an input voltage of 10 V and we chose to define the flow-gain matrix as

$$\mathbf{k}_{SV} = \frac{0.038\, m^3}{60\, s\ \ 10\, V} \begin{bmatrix} 1 & 0 \\ 0 & 1 \end{bmatrix} = \begin{bmatrix} 6.333 \cdot 10^{-5} & 0 \\ 0 & 6.333 \cdot 10^{-5} \end{bmatrix} \ \frac{m^3}{s\ V} \tag{97}$$

Finally, assuming for this example that the displacements of the pistons were equal to the displacement of the specimen, the transformation matrix introduced in expression (54) was

$$T = \begin{bmatrix} 1 \\ 1 \end{bmatrix} \tag{98}$$

4.3.2 Analytical parameters determined after comparison with the experiment results

The parameters contained in this subsection were determined by trial and error in order to optimise manually the matching of experimental and analytical results. Such graphical comparison is shown in the next subsection for the optimised values of these parameters.

The oil column stiffness matrix for the actuators was estimated as

$$\mathbf{k}_{oil} = \begin{bmatrix} 2.9 \cdot 10^7 & 0 \\ 0 & 2.9 \cdot 10^7 \end{bmatrix} \ N/m \tag{99}$$

Note that, even though expressions such as (19) or (20) could have been used to derive a value for this parameter, by using the experimental estimation, we are giving to this parameter an effective value that may take into account some effects ─not covered by the original formulae (19) or (20)─ such as effective values of the bulk modulus of the oil, volume that is submitted to compression, flexibility of other parts in the actuator, etc…

The time constant for the leakage at the actuators was also estimated as

$$\boldsymbol{\tau}_{lea} = \begin{bmatrix} 0.83 & 0 \\ 0 & 0.83 \end{bmatrix} \ s \tag{100}$$

and the viscous-equivalent internal damping of the pistons as

$$\mathbf{c}_{pis} = \begin{bmatrix} 1.2 \cdot 10^5 & 0 \\ 0 & 1.2 \cdot 10^5 \end{bmatrix} \quad Ns/m \tag{101}$$

Finally, the output sensitivities of the controller were estimated as

$$\mathbf{k}_{con} = \begin{bmatrix} 1.964 & 0 \\ 0 & 1.964 \end{bmatrix} \quad V \tag{102}$$

It should be noted that it would have been also possible to give a nominal value to this output sensitivities of the controller and then make the estimation of the servo-valve flow gains (97) from the experimental results. The product of both values should have been always the same.

4.3.3 Comparison of analytical and experimental FRFs

A MATLAB function called "psdss" had been already written able to construct the constant matrices (87) from the given values of the parameters of the model. For this 1-DoF example we decided to use directly that function instead of writing another specific function for the matrices of the equations of the control system (77). Then, for obtaining the FRFs at every frequency, for an input (86) of an arbitrary complex unit harmonic

$$\mathbf{u}(t) = \left[\mathbf{f}_{INP}(t)\right] = \left[1\right] e^{j\omega t} \quad ; \quad j = \sqrt{-1} \tag{103}$$

the state space equation (85) was solved as

$$\mathbf{x}(t) = \left[\mathbf{X}\right]_\omega e^{j\omega t} = \left[\left(j\omega \mathbf{I} - \mathbf{A} \right)^{-1} \mathbf{B} \left[1\right] \right] e^{j\omega t} \tag{104}$$

where, according to definition (86), the vector

$$\left[\mathbf{X}\right]_\omega = \begin{bmatrix} \mathrm{D}_{sp}^r \\ \mathrm{V}_{sp}^r \\ \mathrm{D}_{sp} \\ \mathrm{V}_{sp} \\ \mathrm{F}_P \\ \mathrm{E}_I \end{bmatrix}_\omega \tag{105}$$

contains the complex amplitudes of all the state variables of the model corresponding to excitation (103). Then, the value of the closed-loop FRF of the control system at that frequency is obtained as the complex ratio between the reference and the measured displacements

$$H(\omega) = \frac{\left[\mathrm{D}_{sp}\right]_\omega}{\left[\mathrm{D}_{sp}^r\right]_\omega} \tag{106}$$

while the open-loop FRF is computed as the complex ratio between the error and the measured displacement

$$G(\omega) = \frac{\left[\mathrm{D}_{sp}\right]_{\omega}}{\left[\mathrm{E}_{sp}\right]_{\omega}} = \frac{\left[\mathrm{D}_{sp}\right]_{\omega}}{\left[\mathrm{D}^{r}_{sp}\right]_{\omega} - \left[\mathrm{D}_{sp}\right]_{\omega}} = \frac{H(\omega)}{1 - H(\omega)} \tag{107}$$

However, if the specimen would have had more that 1 DoF, these FRFs would have been matrices instead of scalars and they should have been derived directly by programming the solution of equations (77) in a specific function.

Then, the parameters values given in the two previous subsections were used to build the constant matrices (87), solve the state variables (104) and obtain the FRFs (106) and (107).

Figure 20 and ***Figure 21*** correspond to the cases of runs 11, 10 and 16 in Table 1, for which the nominal amplitude was 6 mm and the P parameter was 0.2, while the I parameter changed from run to run. Similarly to ***Figure 7*** and ***Figure 8***, the closed-loop and open-loop experimental FRFs are again plotted (with a dashed line), but adding this time for every value of the I parameter the analytical curve (continuous line with the respective colour). In the closed-loop graphs in ***Figure 20*** we have used linear scale of frequency and amplitude in order to have a better view of the frequencies higher than 1 Hz. In the open-loop graphs in ***Figure 21*** we have used logaritmic scale of frequency and amplitude in order to have a better view of the frequencies lower than 1 Hz. Either for the closed and the open-loop graphs, the obtained matching of experimental and analytical curves is acceptable for frequencies up to more or less 5 Hz, regarding amplitude and up to 1.5 Hz, regarding the phase.

Figure 22 and ***Figure 23*** correspond to cases of runs 16, 12 and 13 in Table 1, for which the I parameter was 500 and the P parameter was 0.2, while the nominal amplitude changed from run to run. Because of the linearity of the model, the amplitude of the displacement cannot modify the analytical FRFs. The obtained matching of experimental and analytical curves is similar to the ones in the previous graphs. However, the smallest amplitude (1 mm) run has an earlier deterioration of the quality in the data due to the stronger effect of the measurement errors at high frequencies.

Finally, ***Figure 24*** and ***Figure 25*** correspond to cases of runs 14, 16, 15, 8 and 7 in Table 1, for which the nominal amplitude was 6 mm and the I parameter was 500, while the P parameter changed from run to run. The obtained experimental-analytical matching is similar to the one in the previous graphs.

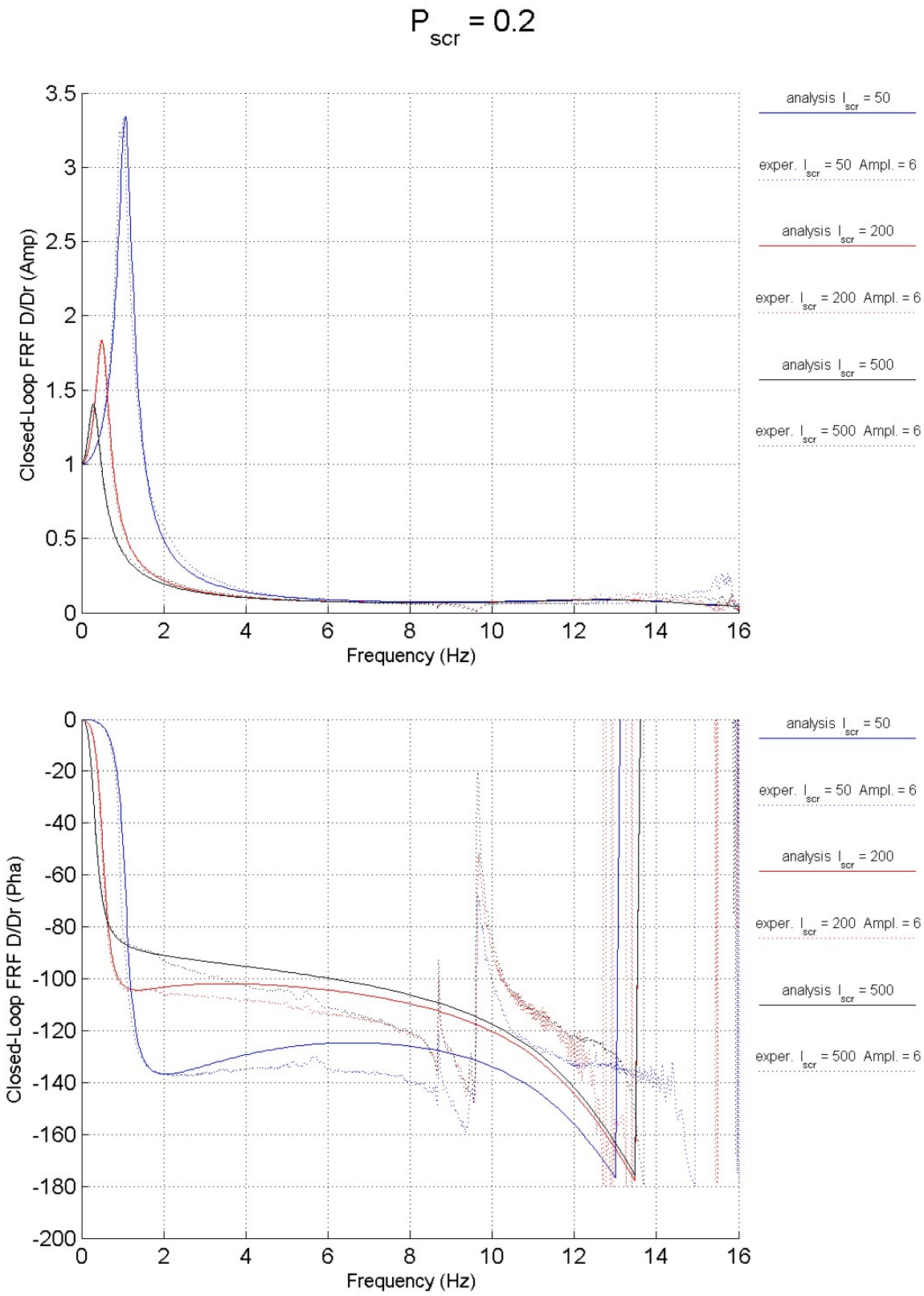

Figure 20. Sine chirp test. Experimental-analytical comparison of closed-loop FRFs for varying I parameter.

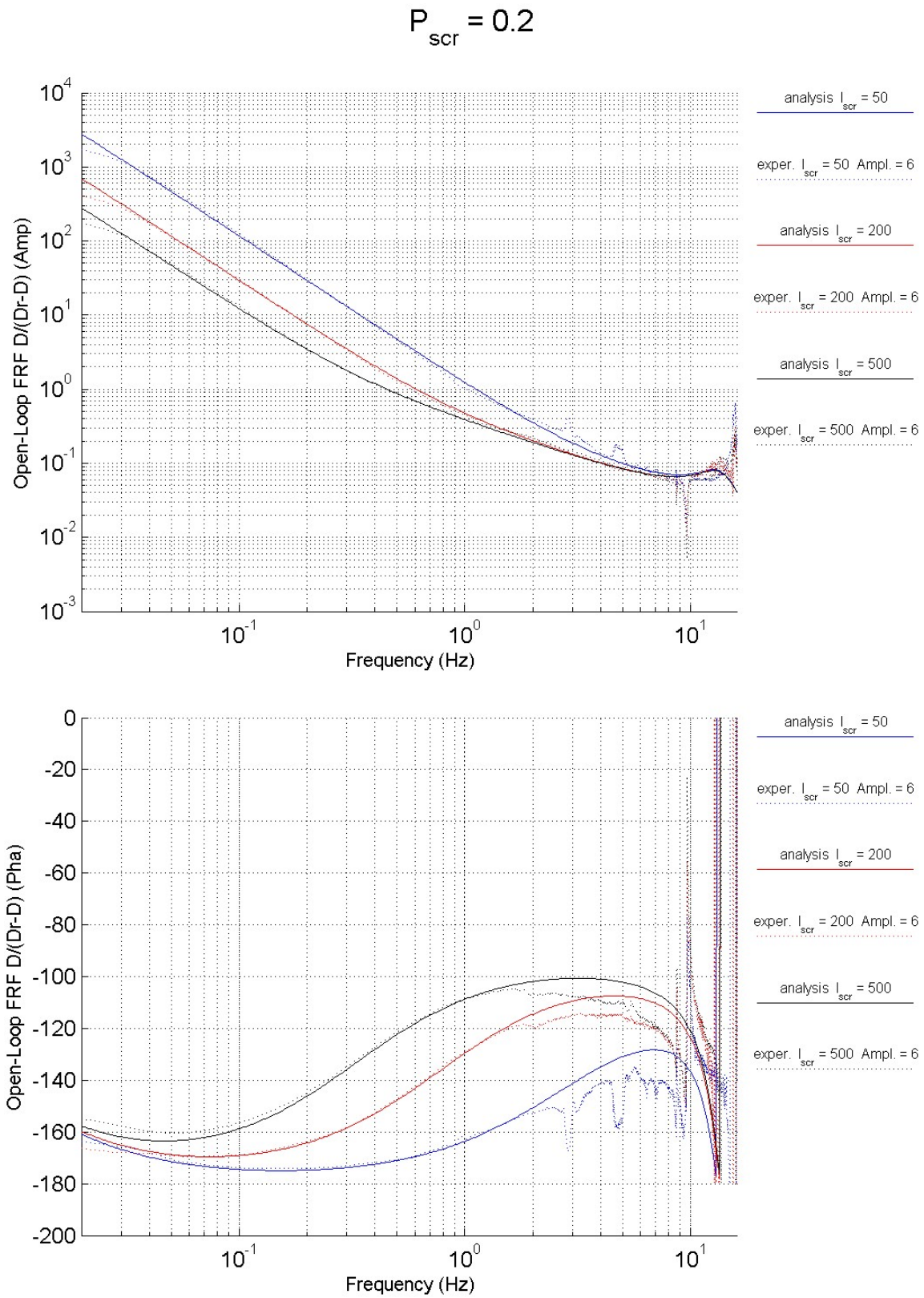

Figure 21. Sine chirp test. Experimental-analytical comparison of open-loop FRFs for varying I parameter.

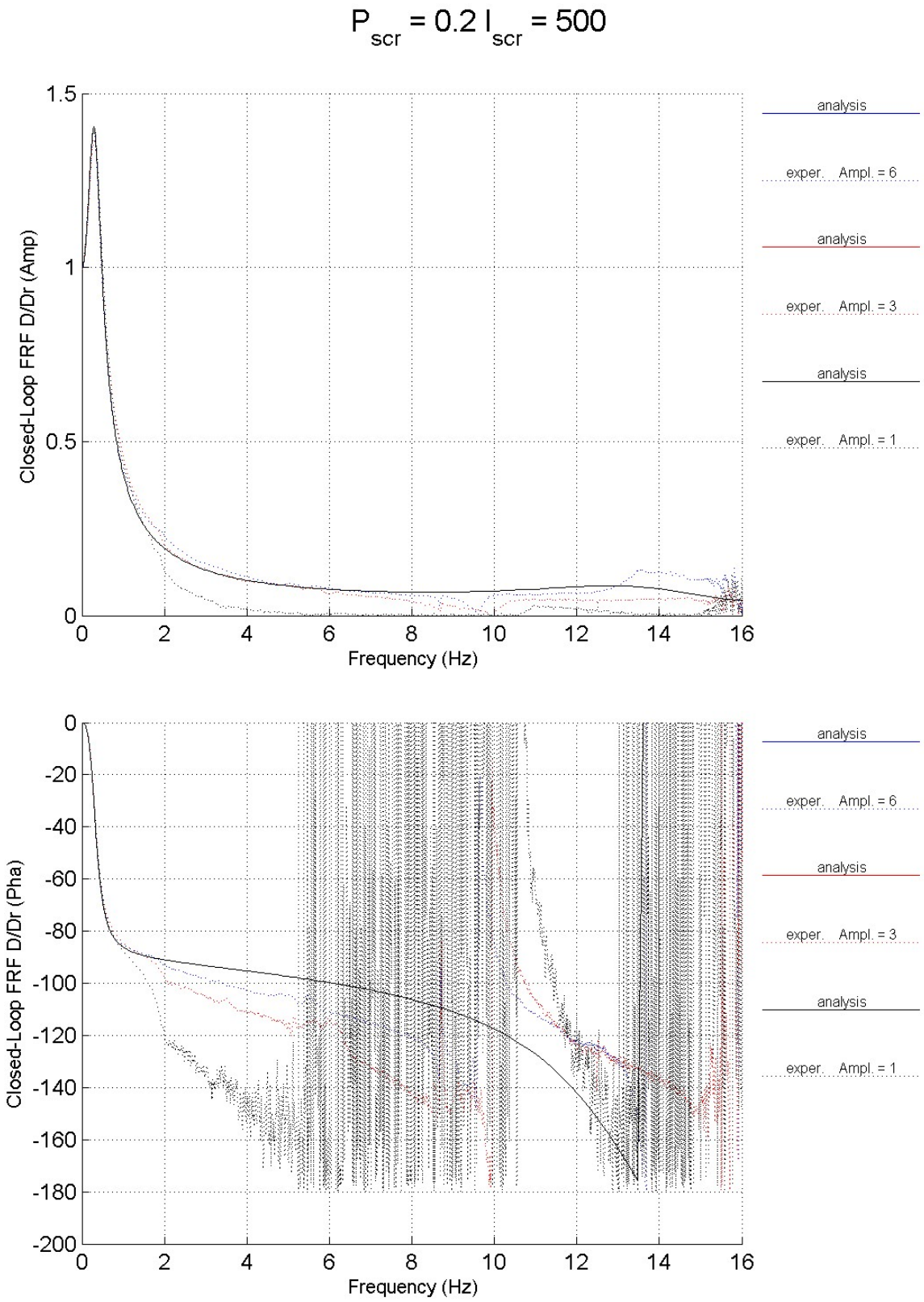

Figure 22. Sine chirp test. Experimental-analytical comparison of closed-loop FRFs for varying amplitude.

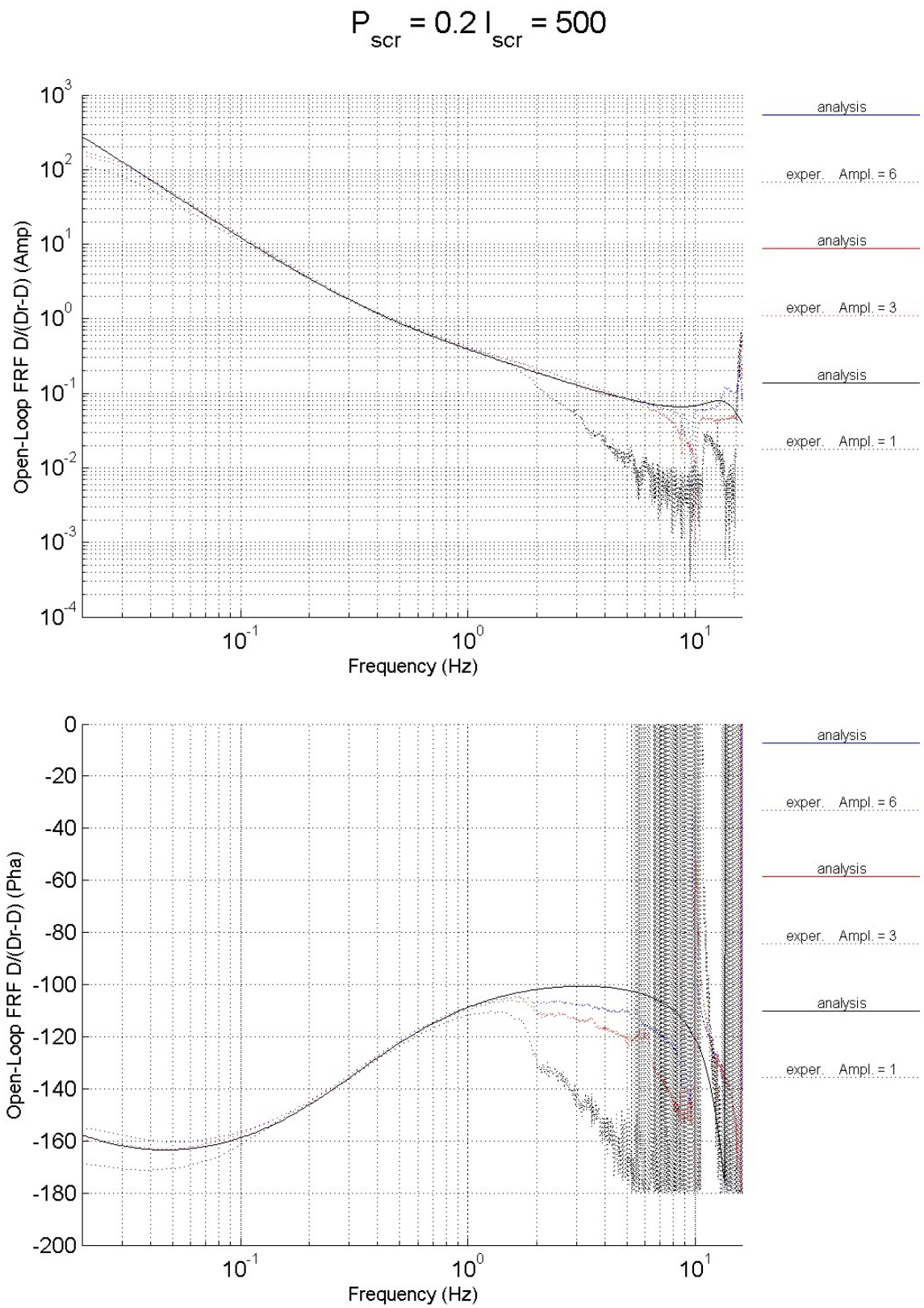

Figure 23. Sine chirp test. Experimental-analytical comparison of open-loop FRFs for varying amplitude.

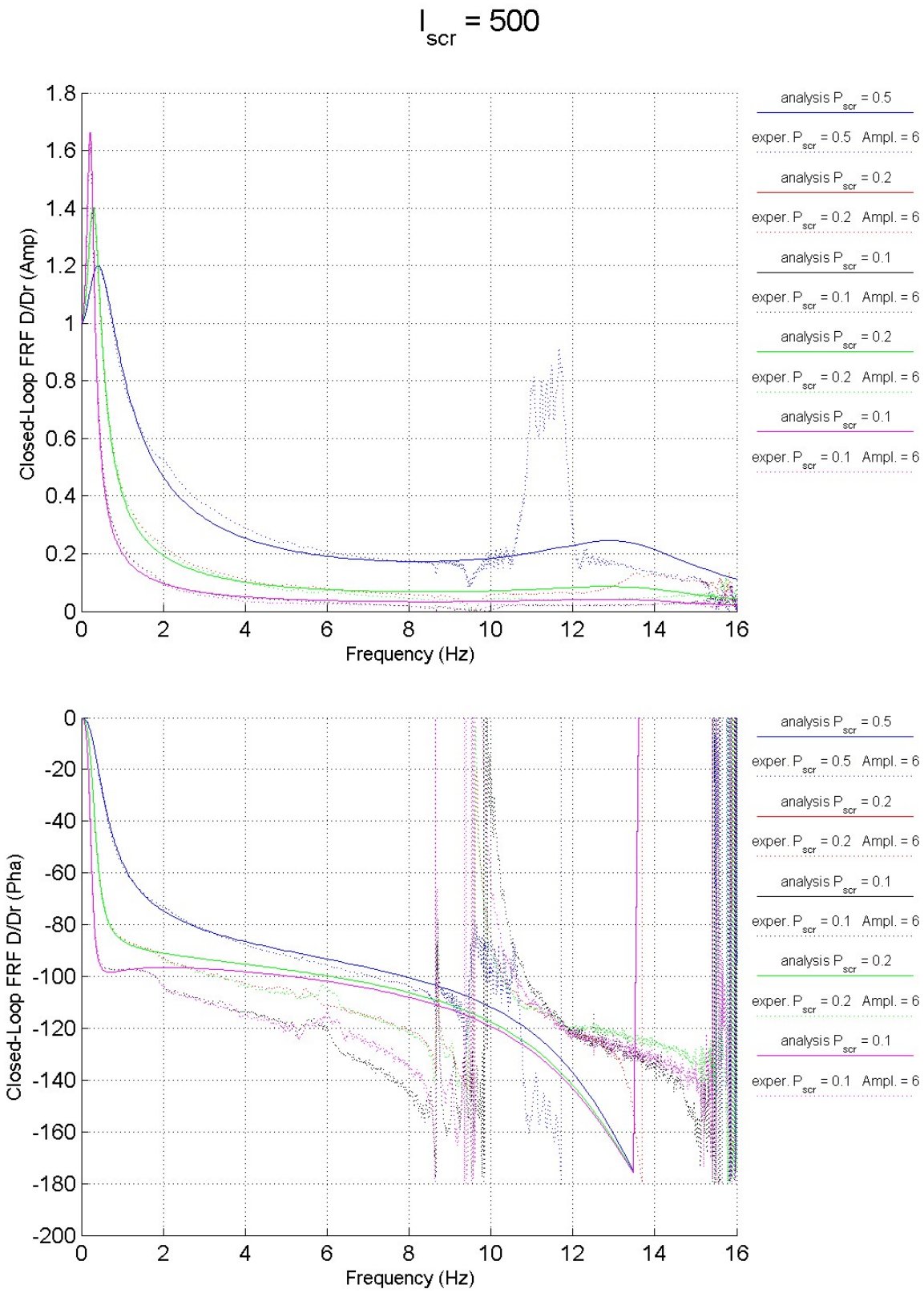

Figure 24. Sine chirp test. Experimental-analytical comparison of closed-loop FRFs for varying P parameter.

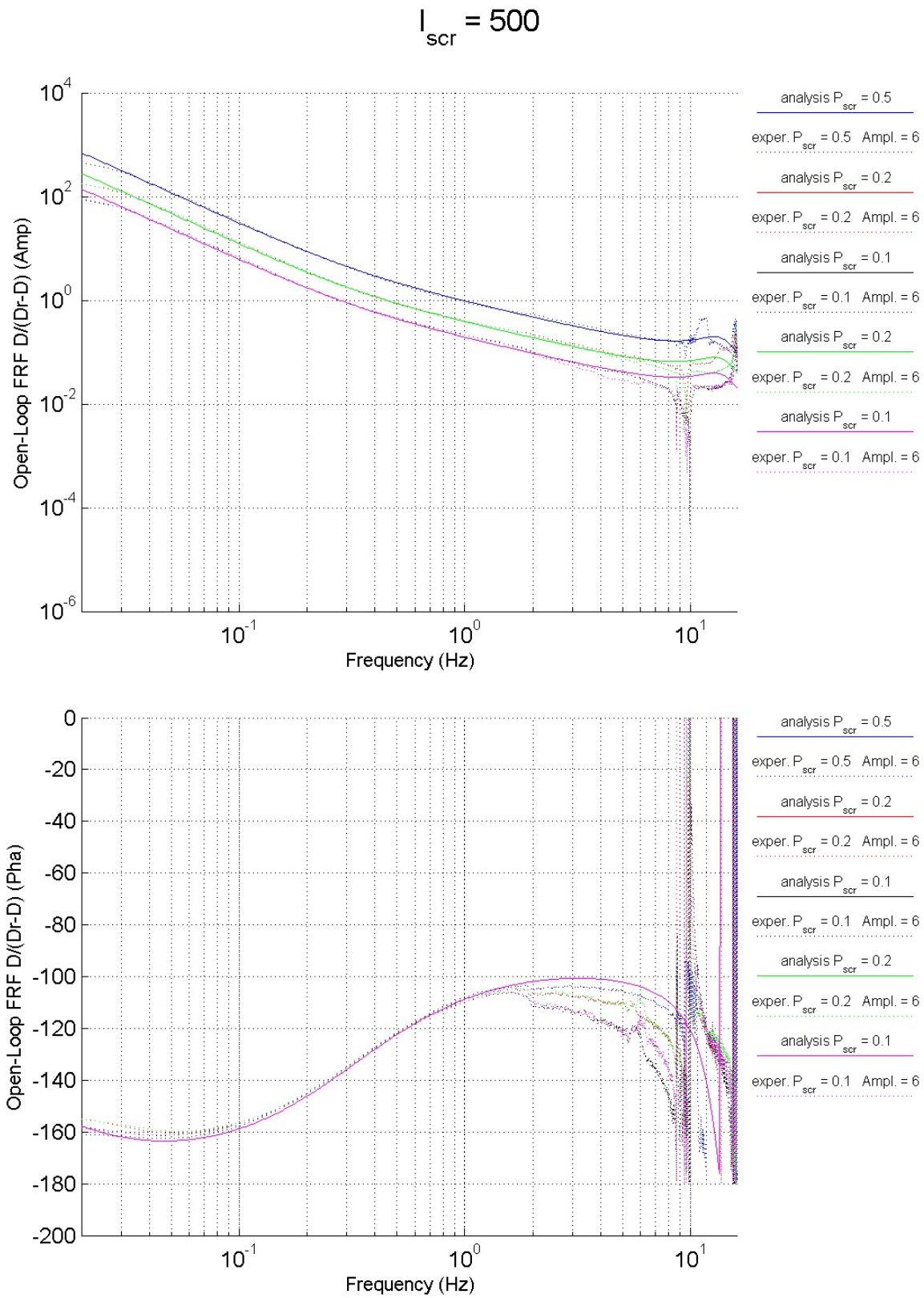

Figure 25. Sine chirp test. Experimental-analytical comparison of open-loop FRFs for varying P parameter.

5 CONCLUSIONS

A linear model of the ELSA continuous PsD testing has been developed that includes the most important aspects of the control system regarding the quality of the tests. The model of the hydraulic actuators is done with symmetric pistons and considers the compressibility of the oil, the leakage between both chambers and the friction of the piston in the cylinder. Since the model is developed for simulating the expected phenomena in slow speed tests, it should be accurate only for low frequencies and, thus, the servo-valves are considered perfectly proportional. The model includes PID control with additional feed-forward and differential pressure terms and is able to deal with several DoFs in the specimen controlled by several actuators.

Multi-frequency tests performed on a 1-DoF steel frame specimen, controlled by two parallel actuators, have provided the measurements for the estimation of the control system FRFs for several displacement amplitudes as well as for several values of the proportional and integral gains of the controllers. The coherence of the obtained FRFs is considered excellent for frequencies up to at least 1.5 Hz. Then, the analytical FRFs obtained by the linear model had been compared with the experimental ones obtaining also a good matching of the curves for that low band of frequencies. This result was got when some of the parameters of the model, such as the oil column stiffness, the leakage constant and the piston damping, were tuned manually.

This analytical model is expected to be used for several purposes such as:

- Parametric studies on the testing set-ups that may help to understand how to optimise the quality of the tests.
- Study of improved alternative control algorithms.
- Study of alternative hybrid testing techniques.

6 ACKNOWLEDGEMENT

The work presented in this paper was partially funded by the European Commission through the SAFECONSTRUCT institutional action n. 32003 of the IPSC of the JRC. The authors acknowledge all the collaboration given by all the colleagues of ELSA.

7 REFERENCES

Avitabile, P. [2005] “Modal space: I know that certain shaker excitations have different characteristics, but which is the best to use?”, Experimental Techniques 29 (2), pp. 15-16

Bairrao, R., Bursi, O., Carydis, P., Magonette, G., Mouzakis, H., Tirelli, D. and Williams M. [2004] “Benchmark testing and performance comparison of shaking tables and reaction walls” Proc. of the 13th World Conference on Earthquake Engineering, Vancouver, Paper N. 441.

Conte, J. P. and Trombetti, T. L. [2000] “Linear dynamic modeling of a uni-axial servo-Hydraulic shaking table system”, Earthquake Engineering & Structural Dynamics, 29, 1375-1404.

Ewins, D. J. [1984] Modal Testing: Theory and Practice, Taunton Research Studies Press.

Hayes, M. H., [1996] Statistical Digital Signal Processing and Modelling, John Wiley.

Knohl, T., Unbehauen, H. [2000] “Adaptive position control of electrohydraulic servo systems using ANN”, Mechatronics 10 (1-2), pp. 127-143.

Magonette, G., Pegon, P., Molina, F. J. and Buchet, Ph. [1998] "Development of fast continuous substructuring tests" Proc. of the 2nd World Conference on Structural Control.

Molina, F. J., Pegon, P. and Verzeletti, G. [1999] "Time-domain identification from seismic pseudodynamic test results on civil engineering specimens" Proc. of the 2nd International Conference on Identification in Engineering Systems, University of Wales Swansea.

Molina, F. J., Magonette, G. and Pegon, P., [2002] "Assessment of systematic experimental errors in pseudodynamic tests" Proc. of the 12th European Conference on Earthquake Engineering, Elsevier Science, Paper 525.

Molina, F. J. and Géradin, M. [2007] "Earthquake Engineering experimental research at JRC-ELSA" Proc. of the NATO workshop. Extreme Man-Made and Natural Hazards in Dynamics of Structures, NATO Security through Science Series C: Environmental Security, ed. Ibrahimbegovic, A. and Kozar, I., (Springer), 311-351.

Molina, F. J., Magonette, G., Viaccoz, B. and Geradin, M. [2008] "Apparent damping induced by spurious pitching in shaking-table testing" Earthquake Engineering & Structural Dynamics 37 (1): 103-119. DOI: 10.1002/eqe.747.

Pegon, P., Molina, F. J. and Magonette, G. [2008] "Continuous pseudo-dynamic testing at ELSA" in Hybrid Simulation; Theory, Implementation and Applications, ed. Saouma V.E. and Sivaselvan M. V. (Taylor & Francis/Balkema) 79-88.

Phillips, C. L. and Harbor, R. D., [1999] "Feedback Control Systems" Prentice Hall.

Plummer, A., R. [2008] "A detailed dynamic model of a six-axis shaking table". J Earthquake Eng;12(4):631-62

Shing, P. B. and Mahin, S. A. [1987a] "Cumulative experimental errors in pseudo-dynamic tests" Earthquake Engineering and Structural Dynamics 15, 409-424.

Vidal, V., [2005] "Evaluacion de la calidad y mejora de la experimentacion sismica de estructuras" PhD thesis, Universidad Politecnica de Madrid.

Ziaei, K., Sepehri, N., [2001] "Design of a nonlinear adaptive controller for an electrohydraulic actuator", Journal of Dynamic Systems, Measurement and Control, Transactions of the ASME 123 (3), pp. 449-456

European Commission

EUR 24313 EN **– Joint Research Centre – Institute for the Protection and Security of the Citizen**
Title: Linear Model of a Pseudo-Dynamic Testing System
Authors: F. J. Molina, G. Magonette and B. Viaccoz
Luxembourg: Office for Official Publications of the European Union
2010 – 49 pp. – 21 x 29.7 cm
EUR – Scientific and Technical Research series – ISSN 1018-5593
ISBN 978-92-79-15125-5
DOI 10.2788/82843

Abstract
A linear analytical N-DoF model of a complete pseudo-dynamic testing system is developed and calibrated by means of comparison with experimental results. The model is formulated as a state space equation system by assembling the respective equations for the hydraulic actuators, control law, specimen and testing method. For the case of a 1-DoF steel frame specimen, the control characteristics are experimentally obtained and used for the tuning of the parameters of the model. This model can be useful for understanding and quantitatively predicting distortions of the pseudo-dynamic response due to the presence of control errors as well as for simulating alternative testing methods.

The mission of the JRC is to provide customer-driven scientific and technical support for the conception, development, implementation and monitoring of EU policies. As a service of the European Commission, the JRC functions as a reference centre of science and technology for the Union. Close to the policy-making process, it serves the common interest of the Member States, while being independent of special interests, whether private or national.

LB-NA-24313-EN-C

JRC
EUROPEAN COMMISSION

ISBN 978-92-79-15125-5

Publications Office
Publications.europa.eu